LU TP 12-39

Describing radial patterning and leaf polarity in plants using a model of a dynamic shoot apical meristem with primordia initiation

Master of Science Thesis

Department of Astronomy and Theoretical Physics
Lund University

September 2012

Author: André Larsson
Supervisor: Henrik Jönsson

Lund University
Faculty of Science

Abstract

The initiation of leaf and flower primordia in plants occurs in the shoot apical meristem and results in visible large–scale regular patterns of organs. It has previously been proposed that the initiation of new primordia is triggered by the plant hormone auxin by a mechanism that is confined to the outermost epidermal layer of the meristem. Recent experiments suggest that the genes *KANADI* (*KAN*) and *REVOLUTA* (*REV*), involved in determining the polarity of leaves, might also be involved in the primordia initiation mechanism. Here we introduce and analyse in detail a model which aims to reproduce the distinct KAN and REV pattern as observed in confocal microscopy, along with the dynamics of leaf primordia initiation. In accordance with experimental results, *REV* expression in the meristem is regulated by microRNAs, and a gap consisting of cells expressing neither *KAN* nor *REV* lies in the boundary between regions of *KAN* and *REV* expression. Antagonistic KAN and REV interactions are shown to be sufficient to set a mutually exclusive KAN/REV pattern with a gap. Model predictions suggest a self-activation mechanism for the KAN gene expression. When the model is combined with a hypothesis of active transportation of auxin by polarised PIN1 proteins, a whorled organ pattern was generated. Model considerations points to a need of investigating the signalling pathway between auxin and PIN1 in more detail.

Contents

I Introduction . . . 3
- I.i Symmetries of plants and nature . . . 3
- I.ii The shoot apical meristem and its relation to phyllotaxis . . . 4
- I.iii Studies of plants by means of computer modelling . . . 6
- I.iv Final model used in this report . . . 7

II Results and Discussion . . . 8
- II.i The REV and miRNA model interactions form a bistable switch . . . 8
- II.ii A central source of auxin is sufficient to break the symmetry . . . 11
- II.iii A central zone anchor results in a more stable model compared to a PZ anchor model . . . 15
- II.iv The desired cell differentiation states can be obtained by antagonistic interactions between KAN and REV . . . 17
- II.v Combining the KAN/REV network with a regulation of miRNAs also results in a model capable of recreating the cell states required for radial patterning . . . 21
- II.vi KAN mutants motivates an inhibition of REV by KAN . . . 23
- II.vii miRNA promoter mutants perturb model species expressions . . . 23
- II.viii REV mutants suggests some additional robustness factor in cells expressing KAN . . . 24
- II.ix KAN self-activation can result in a more robust model and a better gap between KAN and REV . . . 27
- II.x A relevant auxin distribution in the L1 layer can be created by a PIN1 polarisation transport mechanism together with a central signal . . . 28
- II.xi Model predicts central/peripheral patterning in the L1 layer and permits organ initiation . . . 30

III Conclusions and Future Work . . . 32

IV Methods . . . 33
- IV.i Mathematical modelling . . . 33
- IV.ii Simulation software . . . 37
- IV.iii Analytical solutions and nullclines . . . 37
- IV.iv Bifurcation analysis . . . 38
- IV.v Parameter optimisations . . . 39
- IV.vi Sensitivity analysis . . . 41
- IV.vii Principal component analysis . . . 42
- IV.viii Mutants . . . 42

V Appendix . . . 43

V.i Analytical solution of the KAN/REV sub network 43
V.ii Relationship between networks with/without a KAN self-activation mechanism 45
V.iii Reducing the number of parameters in a biological system 48
V.iv Equations of the anchor models 51
V.v Equations of the single cell KAN/REV network 53
V.vi Equations of the single cell full model 54
V.vii Gene expressions of the anchor models 55
V.viii Model mutants gene expressions 56
V.ix Parameter distributions 60
V.x Parameter values used in bifurcation analysis 64
V.xi Parameter values used for the *in silico* experiments 65
VI Acknowledgements 65

References **66**

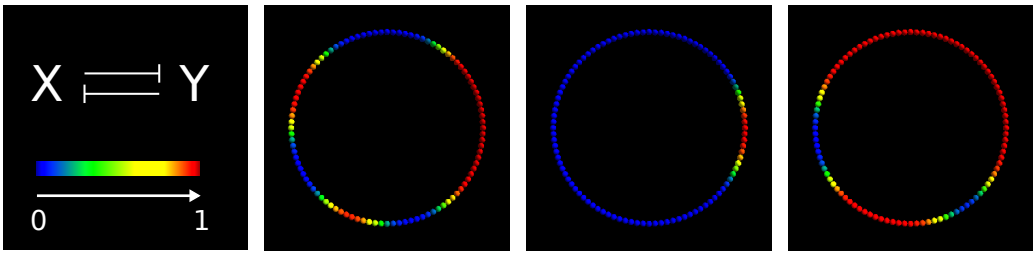

(a) (b) (c) (d)

Figure 1: Examples of patterns resulting from a simple gene regulatory network (GRN). **(a)** The GRN and the colour scale used. The network forms a positive feedback loop/bistable switch and the template allows for diffusion of both species. **(b)**–**(d)** The concentration of the species X at equilibrium in a circle of cells, where the cells are initiated with different random X, Y concentrations. Due to the symmetry of the reactions, the pattern of species Y will be the inverse of that of X.

I Introduction

I.i Symmetries of plants and nature

Patterns and repeated structures are a commonly recurring theme in nature. It has been shown that a wide array of complex patterns can be generated from a set of simple rules written as differential equations [Turing, 1952]. Equations of this type are used to describe reaction–diffusion systems, e.g., systems with chemical reactions and passive transport (diffusion) of molecules. Different reaction rates or reaction types give rise to different patterns. In effect this means that the patterns described mathematically can be realised by nature using reactions between chemical compounds. There has been several proposals of how this might occur, one set of approaches involves a weak initial pattern that is amplified by various feedback mechanisms [Gierer and Meinhardt, 1972, Turing, 1952] (Figure 1).

Specifically, plants exhibit patterns in the form of e.g., distichous, decussate and spiral leaf arrangements. The arrangement of leaves on a plant stem is known as phyllotaxis. Spiral patterns as seen in e.g., sunflowers and pine cones has been shown to relate to the Fibonacci series and the golden angle. Organs in sunflowers and pine cones arrange to form both left– and right–handed spirals known as parastichies. The number of parastichies in each direction are found to be consecutive Fibonacci numbers, [Church, 1904, Adler, 1974, Douady and Couder, 1992] and the angle between a newly formed organ and the previous one is close to the golden angle.

Various mechanisms giving rise to the symmetries of phyllotaxis have been proposed, many of them relating back to the simple result that new leaf primordia is created at the spot furthest away from old primordia [Hofmeister, 1868,Snow and Snow, 1932]. This has led to suggestions that primordia in plants generate some sort of inhibition field [Schoute, 1913] that push new primordia away from previously created ones. Another idea is that new primordia is automatically created when a certain amount of primordia-free space is available [Iterson, 1907]. It has been shown that a model with a growing apex coupled to a spacing mechanism is sufficient to recreate the spiral patterns observed in

nature [Mitchison, 1977, Douady and Couder, 1992], regardless of the details behind the spacing mechanism. The relation to the Fibonacci numbers also seems to be a property of spirals forming in this manner. However, the exact nature and details of how primordia formation is triggered and how the primordia is positioned is still an open question.

I.ii The shoot apical meristem and its relation to phyllotaxis

New leaves and organs are formed in the shoot apical meristem (SAM), located at the apex of the growing plant. A constant population of stem cells in the central zone (CZ) of the SAM is created and maintained by cells in the organising center (OZ). The constant cell growth and cell division in the meristem results in a flow of cells away from the center towards the peripheral zone (PZ). As the cells move out to the PZ, they differentiate into more specialised cell types.

It is known that the presence of the plant hormone auxin is necessary for leaves to form correctly [Reinhardt et al., 2003]. Further, it is shown that cells differentiating into leaf primordia are preceded by a high level of auxin [Benková et al., 2003, Heisler et al., 2005]. These results suggests that auxin acts as an activating signal that determines where and when leaf primordia are formed. The distribution of auxin within the SAM is seen to follow a spacing mechanism, with new peaks of auxin appearing at the spot furthest away from old primordia. This distribution of auxin is influenced by auxin influx and efflux mediators such as the PINFORMED1 (PIN1) efflux mediators [Gälweiler et al., 1998] and the AUXIN1 (AUX1) influx mediators [Yang et al., 2006].

Auxin might be present in the CZ. There are some uncertainty in the measurements of auxin expression; although the auxin-responsive transcriptional reporter DR5 shows no sign of auxin in the CZ, other experiments have found evidence suggesting that DR5 might give a skewed picture [de Reuille et al., 2006]. A new reporter has recently been introduced, suggesting a different pattern of auxin [Vernoux et al., 2011, Brunoud et al., 2012] where auxin is present in the CZ.

The leaf founding cells are defined by the auxin peaks in the meristem, but the polarity of the leaf must also be laid out. Leaves have distinct upper (adaxial) and lower (abaxial) sides. The adaxial side of the leaf faces the sun and is specialised towards photosynthesis while the shaded abaxial side is geared towards interactions with the atmosphere such as gas or water exchange. In the meristem, cells differentiating to form the abaxial side are seen to express *KANADI* (*KAN*) and *kan* loss–of–function mutants results in adaxialised leaves [Kerstetter et al., 2001, Eshed et al., 2004]. These results leads to the conclusion that the *KAN* gene family expression in a leaf embryo sets the adaxial cell fate. In a similar manner, the expression of class III HD-Zip genes, including the gene *REVOLUTA* (*REV*), is shown to specify adaxial cell fate in the leaf embryo [Otsuga et al., 2001, Emery et al., 2003].

When modelling the mechanisms behind primordia formation it might be sufficient to consider only the epidermal layer of cells in the SAM. This relates to the fact that the meristem is divided into three distinct layers: the epidermal L1, L2 layers (tunica) and the L3 layer (corpus) which is positioned below the tunica [Satina et al., 1940]. Cells in the L1 and L2 layers divide anticlinal, resulting in two independent layers where the cell growth and cell division is confined to two dimensions. Hence there is no movement of cells in or out from the L1 layer. The cells of the L3 layer are free to divide in all three

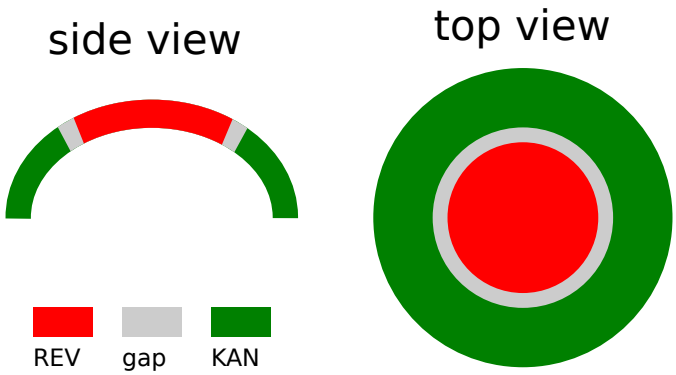

Figure 2: Schematic of how the L1 layer of the SAM is patterned by REVOLUTA (REV) and KANADI (KAN). The gap consists of a line of cells with a low concentration of both KAN and REV. This gap separates the KAN region from the REV region. The REV region roughly coincides with the central zone while the KAN regions approximately coincides with the peripheral zone.

dimensions and thus become less ordered. This separates the L1 and L2 layers from the cells in the L3 layer. Together with experimental evidence and modelling efforts [Bilsborough et al., 2011] this suggests that the L1 layer can be treated independently.

Other players specifying the gene expression pattern are microRNAs (miRNAs) 165 and 166 which are thought to target and down regulate class III HD-Zip genes [Kidner and Martienssen, 2004, Emery et al., 2003]. The miRNAs attach to the transcript of the gene, and inhibits gene expression either by forming an inactive complex with the mRNA, making it unavailable for translation, or by degradation of the mRNA.

Experiments and modelling have revealed common themes in the formation of leaves, vascular tissues, SAM and plant embryos. Vascular tissues are thought to form by a mechanism involving auxin and transportation by polarised PIN1 proteins [Rolland-Lagan and Prusinkiewicz, 2005], the same interactions which are used in models of leaf initiation and positioning in plants. This relates vein formation in leaves to leaf formation in plants. However, the rules and mechanisms that govern the polarisation of the PIN1 proteins by auxin remain disputed. Further, a pattern of KAN and REV is thought to specify the peripheral–central identity of the plant [Izhaki and Bowman, 2007], e.g., REV has been found to be expressed in the CZ of the meristem but not in the PZ [Heisler et al., 2005] (Figure 2). This mimics the patterning of REV and KAN in the leaf, where the pattern determines the adaxial-abaxial identity. These results point towards the possibility of a unifying model for pattern formation in plants.

The outgrowth of primordia has been suggested to occur mainly in the gap between REV and KAN along with a presence of auxin [Yamaguchi et al., 2012]. This would mean an important role for the gap cells, as they would set the position of primordia initiation. The adaxial/abaxial identity could then possibly follow directly from the central/peripheral identity of the meristem.

I.iii Studies of plants by means of computer modelling

Computer models are used to test hypothesis, explain phenomena and to predict new results. The genes and interactions observed in experiments can be merged *in silico* to see if they give a consistent picture of the biology. In a system of several molecular reactions with diffusion and cell growth, computers can successfully be used to find the behaviour of the system whereas an entirely analytical approach often becomes intangible or impossible to follow.

As an example of an early model of plant growth and phyllotaxis, early efforts consisted of e.g., the plant modelled as a half sphere on top of a cylinder, where the cylinder would represent the stem and the half sphere would represent the meristem [Veen and Lindenmayer, 1977]. In this model, an inhibitor was created in the meristem and allowed to diffuse downwards, creating a radially symmetric concentration gradient in the stem. Primordia were allowed to form when this substance had fallen below a certain threshold. The effect was that primordia was initiated at a constant distance from the apex. On top of this an activator or nutrient was homogeneously distributed in the cells. Primordia was then said to require a minimum concentration of this nutrient to form. Primordia further acted as nutrient sinks, in effect creating a field around each primordia where the concentration of nutrient was too low for other primordia to form. This shows in a simple way how a spacing mechanism might be achieved and how primordia can be made to form at a constant distance from the apex. Cell growth were modelled by adding a new row of cells at some specified time interval.

Our knowledge of the players involved at a cellular and molecular level have increased in recent times as new experimental procedures and techniques have become available. Currently work is done on incorporating experimental results into models of phyllotaxis and the SAM, such as the observed correlation between the dynamic distribution of auxin and PIN1 transport proteins [Jönsson et al., 2006, Smith et al., 2006].

Different models of the interactions between auxin and PIN1 have been proposed. One set of models rely on auxin flux feeding back to the permeability of cell membranes, such that a flux of auxin leads to a higher flux of auxin [Mitchison, 1980]. This is reminiscent of how rivers are formed, and these models are often used to explain venation in plants [Fujita and Mochizuki, 2006]. In another set of models the rate of auxin flux is determined by the auxin concentrations in neighbouring cells, such that a high concentration of auxin increases the flux. Models using this interaction have been shown to create patterns and can be used to explain phyllotaxis. Here we will use a concentration-based model where auxin is transported actively with influx and efflux transporters along with diffusion [Jönsson et al., 2006].

The peripheral/central regions of the SAM can be distinguished by the type of genes they express. These genes pattern the SAM into different regions via interactions amongst the genes themselves, forming a multicellular gene regulatory network (GRN). A GRN of the SAM has previously been modelled where *CLAVATA3* is expressed in the CZ and *WUSCHEL* is expressed in the OC [Jönsson et al., 2005, Yadav et al., 2011]. The genetic interactions are modelled either with mass action or enzyme–limited Michaelis–Menten kinetics.

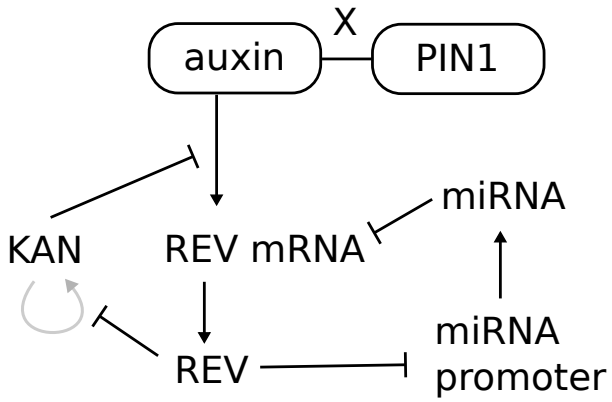

Figure 3: Diagram of the full model, showing how the molecules interacts. KAN and REV are the proteins of *KANADI* and *REVOLUTA* respectively, REV mRNA is the *REVOLUTA* messenger RNA and miRNA represents the microRNAs downregulating REV mRNA. The activations and inhibitions are assumed to be of the Michaelis-Menten type and are modelled by Hill functions, with the exception of the linear activation of REV by REV mRNA. A subnetwork of auxin, PINFORMED1 (PIN1) transport proteins and a proposed signal molecule X creates a dynamic distribution of auxin in the L1 layer. Two variants of the models are used, one where KAN activates itself (grey arrow) and one without this mechanism.

I.iv Final model used in this report

A bottom-up approach was used and models with different sets of reactions have been investigated and later combined into a full model. The final model includes a negative feedback loop between REV and KAN/miRNA, and allows for the initiation of leaf and flower primordia (Figure 3). REV is activated by auxin in the CZ. The distribution of auxin in the meristem is set by a PIN1 transportation model and a smooth source gradient of auxin that peaks in the center and decreases radially outwards. This sets a high auxin concentration in the center and permits peaks of auxin to move outwards to the periphery for primordia initiation, due to cell growth and cell division. The resulting central region of auxin is consistent with the suggestions of recent experiments, where new auxin–responsive markers point to a presence of auxin in CZ [de Reuille et al., 2006, Vernoux et al., 2011].

The central source of auxin is used to activate REV in the CZ. The negative feedback between KAN and REV leads to a high *KAN* expression in the PZ where the *REV* expression is low and vice versa. *REV* is also regulated with miRNAs. All reactions occur on a 2D template admitting cell growth and proliferation, representing the L1 layer of the meristem.

II Results and Discussion

II.i The REV and miRNA model interactions form a bistable switch

Cells are found to be in either a KAN or a REV state, meaning that these genes are not simultaneously expressed within one cell. This suggests a negative feedback mechanism between these genes, resulting in the genes being mutually exclusive. Further, miRNAs have been found to be present in the periphery together with KAN and function to downregulate the *REV* expression [Kidner and Martienssen, 2004, Emery et al., 2003]. A simple picture of the situation can be obtained by treating KAN/miRNA as one unit that interacts with REV to form a negative feedback loop. We want a model behaviour where the species REV and KAN/miRNA become mutually exclusive, and use this to set the peripheral/central identity of the SAM as well as the adaxial/abaxial polarity of new organs.

First of all a GRN capable of creating all of the cell states of the system must be specified (Figure 4, Table 1). Focus will be on recreating the mutually exclusive KAN/REV pattern. The role of auxin will be introduced later on. For now, the gap state where neither *KAN* nor *REV* is expressed is not considered in any detail.

We assume that *REV* is degraded by miRNAs, and that there is an inhibition of the miRNA promoter by REV (Figure 5). These reactions are sufficient to form a bistable switch. By setting the parameters of the models to reasonable values, this network can be made to allow for two possible states: one state with high REV/low KAN, and one state with low REV/high KAN (Figure 6).

Note that REV is only regulated by the miRNAs. The miRNAs are modelled to increase of the rate of degradation of the gene rather than to decrease the production of the gene. Still, it is possible to create a bistable switch with the miRNA mechanism. This is in contrast to efforts where similar behaviour is achieved through transcriptional repression [Gardner et al., 2000].

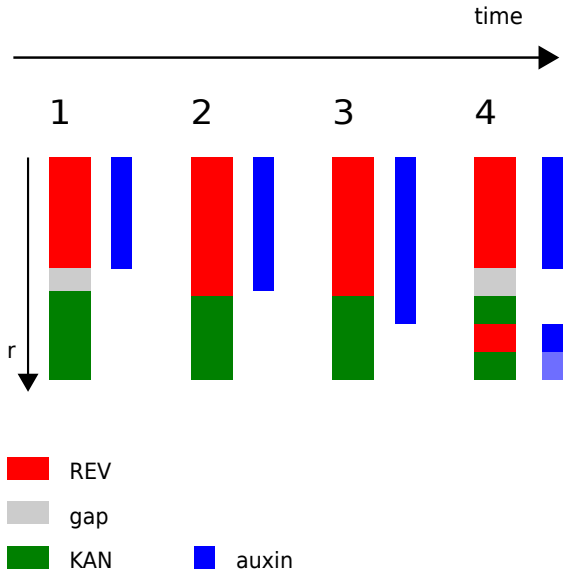

Figure 4: One-dimensional representation of the system. Auxin moves out from the center to form a peak in the periphery. As auxin moves into the gap, *REV* becomes expressed in the gap and the gap disappears.

REV	KAN	auxin	Location
1	0	1	CZ
0	0	0	gap
1	0	1	gap (primordia)
0	1	0	PZ
0	1	1	PZ (primordia)

Table 1: Possible states of different gene expressions and auxin levels, simplified to binary form. In total, there are four different states, two for each level of auxin. Take note that the 'gap (primordia)' is identical to the 'CZ' state. The gene regulatory network should be able to recreate all of these states.

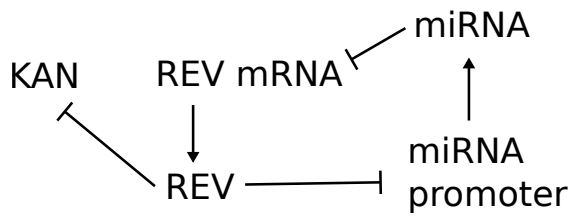

Figure 5: The REV/miRNA gene regulatory network. The REV concentration is completely regulated by the miRNAs and KAN is downstreams of everything.

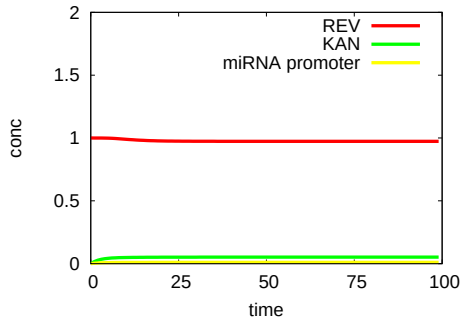

(a) Cell initiated with a high REV concentration and no miRNA/KAN

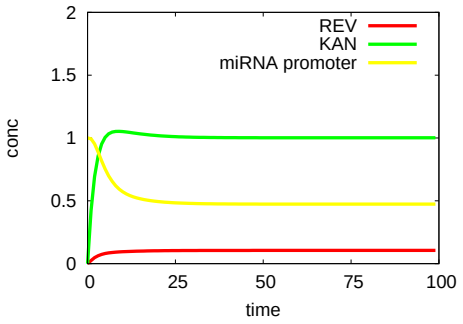

(b) Cell initiated with no REV and a high miRNA concentration

Figure 6: Bistability of the REV/miRNA network. **(a)** The time evolution of the concentrations for a cell initiated with a high REV concentration and KAN/miRNA concentrations of zero. This cell stays in the high REV / low KAN state. **(b)** A cell initiated with a high miRNA concentration and zero REV; this cell switch to a high KAN / low REV state. High concentration is defined as a concentration of 1 (arbitrary scale).

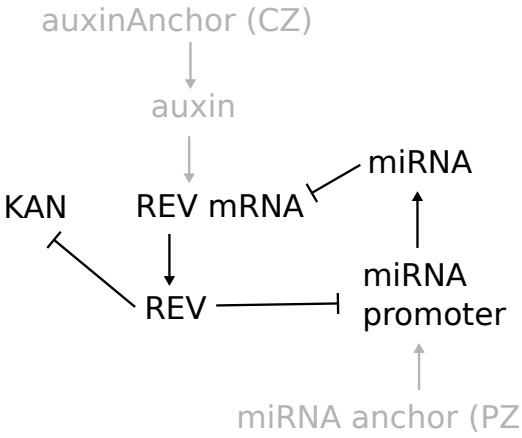

Figure 7: Anchor models. The symmetry is broken either with a miRNA anchor or an auxin anchor, used as a first attempt to create a mutually exclusive KAN/REV pattern. In these models, KAN is completely downstream of everything.

II.ii A central source of auxin is sufficient to break the symmetry

It was not possible to break the symmetry of the 2D model by initiating the system with an uneven distribution of concentrations. This is in contrast to a 1D model where the cells could switch to form a mutually exclusive KAN/REV pattern (cf. Figure 4.1) by using an initial template already containing this pattern. In a 2D model this did not work, probably since different cells will have a different number of neighbours, in effect introducing some noise to the single cell network. This makes it hard to fine-tune the parameters and initial conditions such that each cell remains in its desired state. It was seen that transient mutually exclusive KAN/REV patterns were possible to obtain in the 2D model, but they all eventually broke down into either a homogeneous KAN or REV expression.

Instead, two ways of breaking the symmetry by some external signal was investigated. The first approach involves a constant production of miRNAs (a miRNA anchor) in the periphery to set a miRNA gradient in the L1 layer (Figure 7). This gradient sets the pattern of REV by degrading it in the periphery, and subsequently KAN will be allowed to be expressed there instead. The second sets of approaches uses a radial central source of auxin (an auxin anchor), with different sizes/radii of the source.

It was possible to find parameters in all models resulting in an acceptable pattern but the simulation time and probability of finding good parameters varied between the models (Table 2). It was easier to find good parameters for the model using a large auxin anchor, compared to the model with a smaller anchor. The auxin gradient is steeper close to the anchor and the larger anchor more closely resembles the REV pattern it is supposed to set, meaning that the larger anchor more easily could set the sought pattern. The model with a miRNA anchor was somewhere in between the auxin models in terms of the probability of finding good parameters, but the optimisation procedure was slow compared to the models with auxin anchors.

Models were optimised with cell growth and cell division turned off (Figure 26), but

Model	Fraction f of good parameters	Time per optimisation / T_{miRNA}
miRNA anchor	0.14	1.0
Auxin anchor	0.038	0.32
Auxin large anchor	0.65	0.42

Table 2: Comparisons of parameter optimisations for models with different anchors/sources. The table show how often an optimisation run results in an acceptable set of parameters (Fraction f of good parameters), along with the time for one optimisation run measured relative to the time T_{miRNA} taken for one miRNA anchor model optimisation. The value of f is indicative of how stable the system is; a system with a high fraction means that it is easier to find good solutions. The time per optimisation relates to how hard the system is to solve numerically. It is seen that the model with a large auxin anchor has the highest fraction of good parameters and a decent optimisation time.

the patterns were seen to translate well to templates with cell growth and cell division (Figure 8).

Subtle differences in the recreation of patterns were observed. The model with a smaller auxin anchor had a tendency to have a smaller region of REV than its alternatives, even though the models were optimised against the same pattern. Further, the miRNA anchor model exhibited a softer boundary between the on/off states of the expression levels. This can be explain by the fact that only the outermost cells in the L1 layer produce miRNA, which then diffuses inwards, resulting in a smooth gradient of miRNA in the model. Since the other patterns follow from this smooth miRNA gradient, it is not surprising that the model had a harder time recreating sharp on/off patterns.

Taking everything into account, using a large auxin anchor to set the pattern provided the best solution. It results in a sharp on/off boundary of the concentration gradients and patterns the CZ and PZ correctly. This model also have a high probability of finding good parameters which indicate a higher robustness to parameter variations, and decent simulation times.

The direct biological implication of using a source of auxin to activate REV expression is that auxin must be present in order to have REV expressed. This can be tested by removing or adding auxin to the meristem and see how the REV expression is altered.

The parameter sets are seen to cluster around different points when projected on the first two principal components (Figure 9). The auxin anchor models are separated in the direction of the first principal component. This direction primarily points in the direction of the miRNA parameters, which could mean that role of miRNA is different between these models. Further, the miRNA anchor model is separated from the auxin anchor models in the principal component determined by parameters involved in the production of REV and its degradation by miRNAs. This indicates differences in the strength and importance of the miRNAs between models using a miRNA anchor and models using an auxin anchor.

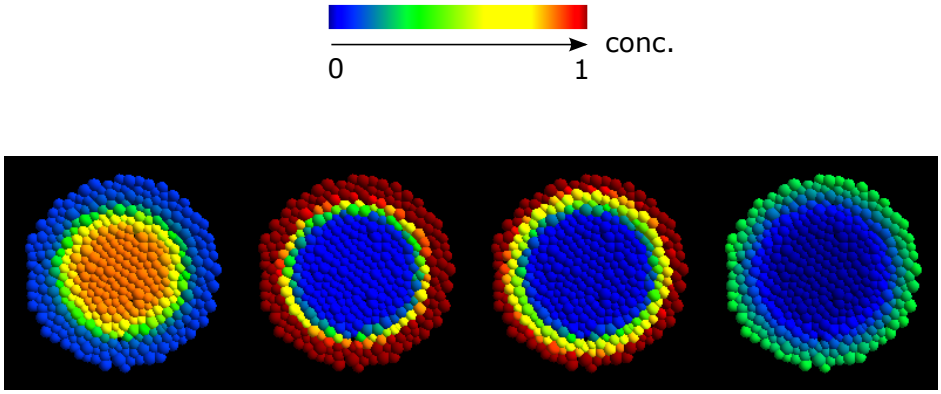

(a) REV **(b)** KAN **(c)** miRNAp **(d)** miRNA

(e) REV **(f)** KAN **(g)** miRNAp **(h)** auxin

(i) REV **(j)** KAN **(k)** miRNAp **(l)** auxin

Figure 8: Concentration levels of different molecules in the anchor models on a template with cell growth and cell division (cf. top view in Figure 2). The models were optimised to recreate a pattern of REVOLUTA (REV), KANADI (KAN) and miRNA promoter (miRNAp). Even though the patterns were optimised on a template without cell growth, they translate well to a growing template. Note differences in the extension and smoothness of the pattern gradients. **(a)** – **(d)** Concentration levels of the miRNA anchor model. **(e)** – **(h)** Concentration levels of the model with a small auxin anchor. **(i)** – **(l)** Concentration levels in the model with a large auxin anchor.

Plot	PC1 important parameters			PC2 important parameters		
(b)	K_{0mip}	Δ_{mi}	d_{mi}	Δ_A	d_a	V_A
	(0.48)	(0.45)	(-0.40)	(-0.59)	(-0.54)	(-0.50)
(c)	V_{mip}	k_{mi}	Δ_{mi}	V_{dRr}	k_{Rr}	K_{2Rr}
	(0.61)	(0.43)	(-0.37)	(-0.53)	(0.47)	(0.36)

(a) Parameters most important for the PCA, and weights shown below the parameter name.

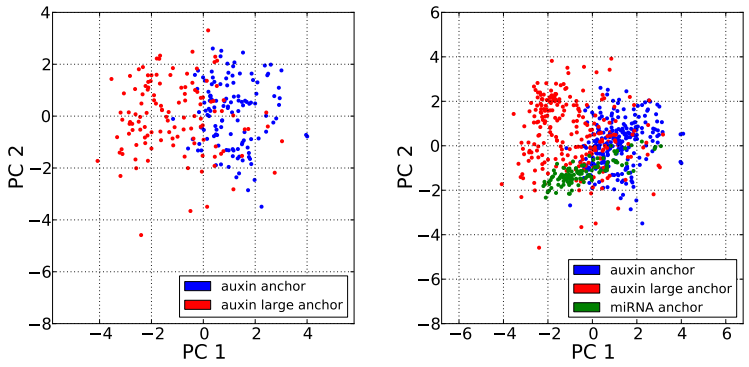

(b) Auxin anchor models (43%)

(c) All three anchor models (38%)

Figure 9: Principal component analysis (PCA) of logarithmised parameters. Each point in the graphs represents a set of parameters and the percentage in the parenthesis is the total explained variance by the two components. We see that the different models form coherent clusters of parameter sets. Further we see that the parameters are centred around different points in the plane of the two first principal components, indicating that the parameters must be set differently depending on the anchor used. The logarithmised parameter sets are normalised to have zero mean and unit variance. **(a)** The three parameters with the largest weight (importance) for each principal component (PC), sorted in descending importance. **(b)** PCA of parameter sets for models using an auxin anchor. **(c)** PCA of parameter sets for models using auxin anchor and miRNA anchor.

II.iii A central zone anchor results in a more stable model compared to a PZ anchor model

A sensitivity analysis was carried out on the anchor models to check how stable they are against perturbations. A small sensitivity can be desirable for a model since this would correspond to a more robust behaviour. The sensitivity analysis is carried out on a selection of the model parameters (Equations 8, 9). Some parameters were excluded since it was considered redundant to check every parameter due the equivalence of some of the model parameters, as shown in Section V.iii.

Generally, the miRNA anchor model is more sensitive to perturbations than the auxin anchor models (Figure 10). This is an argument in favor for the models relying on an auxin anchor and one of the reasons why the miRNA anchor model was discarded from future analysis. A slight change in one of the parameters that are important for the production or degradation of REV (e.g., k_{Rr} or V_{dRr}) is seen to change the total expression significantly, suggesting that the miRNA anchor result in an unstable regulation of REV.

The sign of the sensitivity is positive if a perturbation results in a higher expression compared to the default template, and negative if the perturbation decreases the total expression of a species compared to the template. We see that increasing the production of REV (parameter k_{Rr}) results in a higher expression of REV, and a lower expression of KAN and miRNA, since it acts as an inhibitor for these species. This is as expected, and confirms that the models work as intended.

Further, we see that the sensitivity of the parameters V_K and K_{1K} are zero for the miRNA and REV species. These parameters are related to the production of KAN and it is therefore natural that they do not perturb the expression of other species since KAN is downstreams of everything in these models.

It is of interest to note what happens when changing the parameters of the auxin anchor, since the anchor is supposed to break the symmetry of the model and set the pattern. In the large anchor model, the auxin pattern mirrors that of REV and it can be expected that the REV patterning is more heavily determined by the anchor. The R_A parameter, determining the radius or size of the anchor is seen to have a higher sensitivity with a much larger variance when using a large anchor compared to a smaller one. It seems that the variances of the large anchor model generally is slightly higher than that for the small anchor. This might be due to a larger variety in the quality of the parameters, with different mechanisms setting the pattern of the model. However this possibility has not been investigated further.

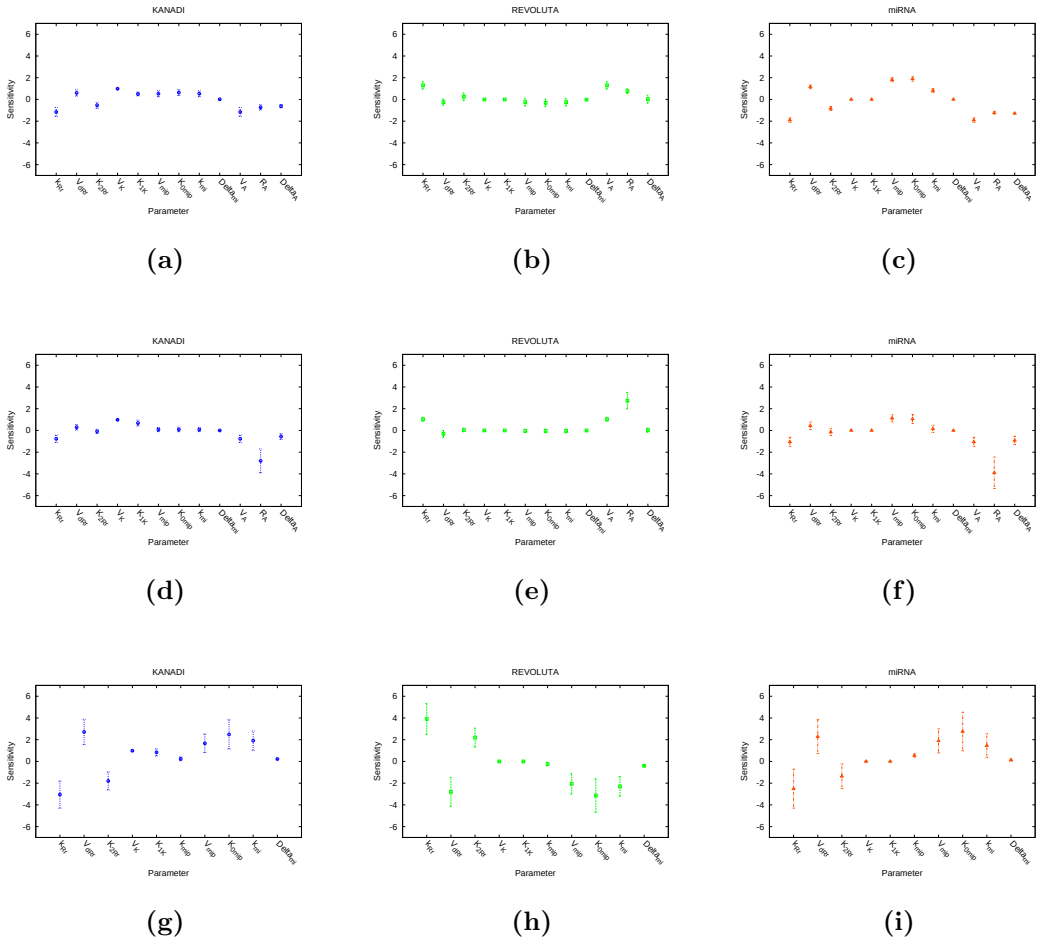

Figure 10: Sensitivity analysis of anchor models. The plotted values show the average sensitivity from ~ 100 sets of parameters, with error bars showing the variance. Many of the parameters of the miRNA anchor model exhibits a high sensitivity (≥ 1) compared to the auxin anchor models, indicating that the miRNA anchor model is unstable. **(a)**–**(c)** The sensitivity values for the model with a small central auxin anchor. **(d)**–**(f)** Sensitivity analysis of the model with a large auxin anchor. **(g)**–**(i)** The sensitivity values for a model with a peripheral miRNA anchor.

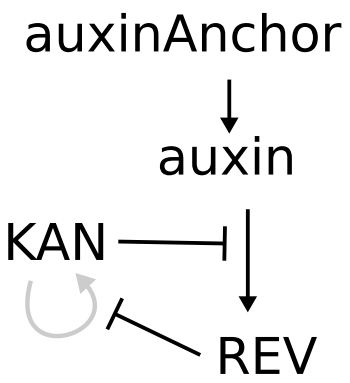

Figure 11: Diagram of the KAN/REV interaction network. This network includes the negative feedback between KANADI and REVOLUTA as well as the activation of REV by auxin.

II.iv The desired cell differentiation states can be obtained by antagonistic interactions between KAN and REV

In the previous sections, miRNAs were used to regulate *REV*. However, it is thought that KAN might also be involved in the regulation of REV. Here the dynamics and interactions of KAN in relation to REV will be investigated in more detail. We suggest a mechanism where KAN inhibits the auxin-mediated activation of REV. A self–activation mechanism of KAN is also introduced, in hopes of making cells with high KAN concentrations more stable against incoming REV cells. This property might be needed in primordia formation in order to allow KAN to be expressed in cells with high auxin and mark the abaxial side of the organs.

To simplify things, a network with only the KAN and REV interactions is modelled (Figure 11). This network consist of a negative feedback loop between KAN and REV, and comes in two variants: the KAN/REV network (KRN) and the KAN/REV network with KAN self-activation (KRN with SA). The equilibrium concentrations of REV/KAN is dependent on the concentration of auxin, but not completely determined by it. It will be shown that one level of auxin might correspond to two different stable equilibrium states of the gene network.

In equations describing chemical reactions, a set of three possible solutions/equilibrium states usually corresponds to two stable equilibria and one unstable. It is therefore of interest to know the number of possible equilibrium states and also how they qualitatively differ from each other. The equilibrium states can be obtained either analytically by assuming equilibrium; setting all time derivatives to zero and solving the equations, or by integrating the system numerically from different initial configurations until it has reached a stable state.

We begin with solving the system analytically. An exact closed–form expression of the equilibrium concentrations was not found, however it was possible to derive equations of the nullclines of the system (Equation 6). The nullclines are the lines that show the concentrations for which the time derivate of a species is zero. Equilibrium states of the system, both the stable and unstable ones, are found where the nullclines intersect. The equilibrium states we want the network to recreate are the cell states observed in experiments (Table 1 and Figure 4).

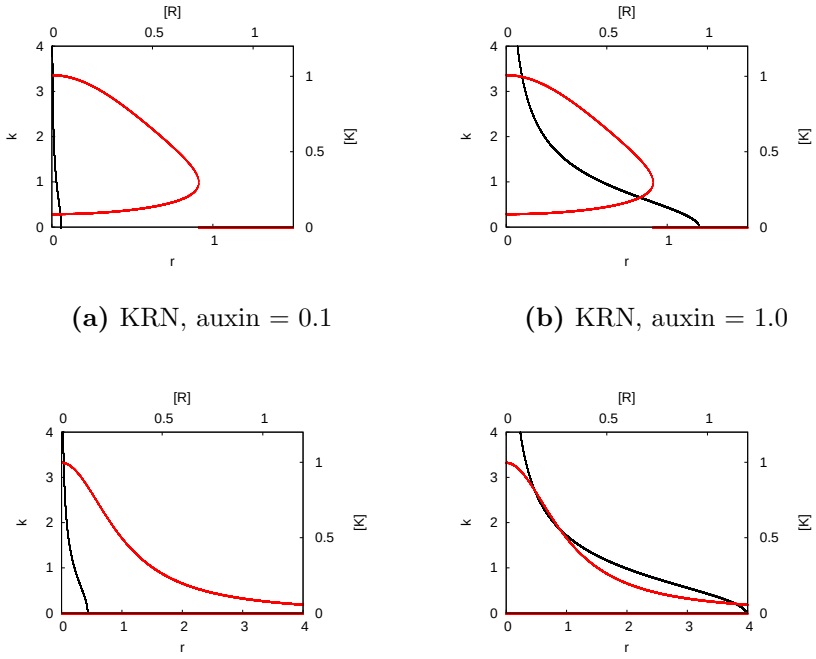

(a) KRN, auxin = 0.1 **(b)** KRN, auxin = 1.0

(c) KRN with SA, auxin = 0.1 **(d)** KRN with SA, auxin = 1.0

Figure 12: REV, KAN nullclines for the KAN/REV network in a single cell. Plots show networks with the KAN self-activation mechanism (KRN with SA) and without the KAN self-activation (KRN). Bottom, left axes shows the dimensionless r, k variables used when solving the system analytically while the top and the right axes shows the [R] and [K] concentrations used in the bifurcation analysis. Remember that the KRN with SA also has a k = 0 nullcline (not plotted here).

The nullclines of the simplified model are plotted for different levels of auxin, to see how the nullclines change and give rise to different points of intersections. This is done for models both with and without self-activation (Figure 12). The KRN with SA is seen to allow two states: one with low REV / high KAN and one with low REV together with a KAN concentration that increases with the level of auxin. The KRN model only has one solution for low levels of auxin, while a higher level of auxin allows for three possible equilibrium states.

The system was also numerically integrated using the software `oscill8` to see how the system responds to different levels of auxin. In effect we are doing a bifurcation analysis on the system with the auxin concentration as the bifurcation parameter. A bifurcation plot shows when and how the solutions of a system diverges in response to changing a parameter. The system is integrated to obtain the equilibrium concentrations of KAN and REV for different concentration of auxin (Figure 13), and we can see how the nature of the equilibrium states changes in response to varying concentrations of auxin.

The bifurcation plots are consistent with the nullcline plots. The network without self-activation have one state with high KAN/low REV expression and another state

with low KAN/increasing REV expressions. In the network with self-activation, there is only one equilibrium state at low levels of auxin, while a higher level of auxin allows for three equilibria of which two are stable.

It can be seen that the main difference between models with and without the self-activation mechanisms is that the self–activation network is monostable for low levels of auxin. Note that the robustness of the models is hard to tell from the plots. However, some comments can be made. The thin lines in the bifurcation plots are unstable equilibria, meaning that a system initiated at or near these concentrations will move away from this point and instead move towards a stable equilibrium. Hence, cells with KAN (REV) concentrations below the thin line will move to the KAN (REV) low state, while cells initiated with concentrations above this line will move to the KAN (REV) high state. Although this is a simplification of the behaviour (since in reality the behaviour of the system depends on both initial concentrations), it still gives some idea of how the system is expected to behave.

The bifurcation analysis shows that the network should be able to create the necessary dynamics. Cells switch between different states as they move from the CZ across the gap and into the PZ. In the CZ, there is a high concentration of auxin and REV while KAN is only weakly expressed. When the cell moves in to the gap, the level of auxin and REV decreases, while the concentration of KAN increases. Here, it can be seen that decreasing the concentration of auxin from 2 to 0.4, the high REV expression drops with about a factor ten, while the KAN expression remains low despite a slight increase in its expression (Figure 13). The end result is a low KAN / low REV state in the gap. As the cell move out from the gap to the PZ, auxin decreases even more. At very low levels of auxin only the high KAN / low REV is available; this is the state PZ cells should be in. Hence this network should be able to explain the central/peripheral patterning in a growing meristem.

Primordia is here marked with auxin while adaxial/abaxial patterning is marked by REV/KAN. Regions of primordia formation can therefore be expected to include cells with high auxin/high REV and cells with high auxin/high KAN. Bifurcation analysis show that both of these states are available in the model, as long as the auxin concentration does not become to high (Figure 13).

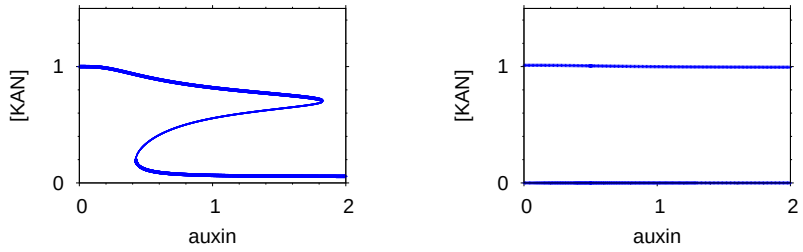

(a) KAN, no SA

(b) KAN, SA

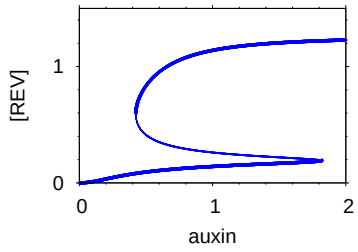

(c) REV, no SA

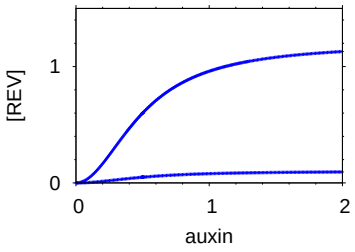

(d) REV, SA

Figure 13: Bifurcation plots with auxin as a parameter of the KAN/REV network (KRN) with KAN self-activation (SA) and without KAN self-activation (no SA). Thick lines show stable equilibria while thin lines show unstable equilibria. In the plots, high KAN values and low REV values belong to the same state, and vice versa. This can be verified by comparing these with the nullclines of the model (Figure 12).

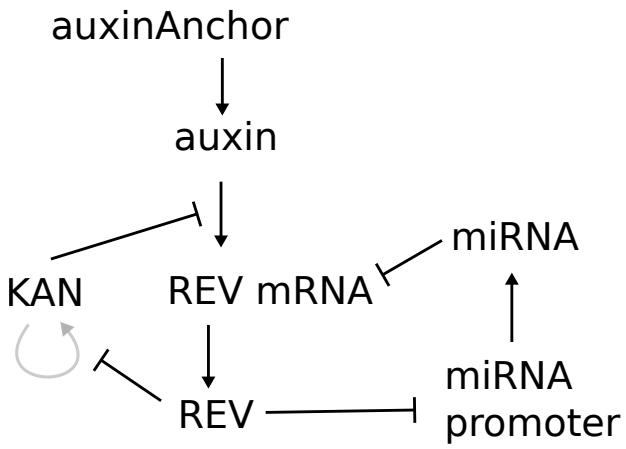

Figure 14: Diagram of model where REV is regulated by both miRNAs and KAN. *REV* is activated by auxin which in turn is set by an anchor. Two variants of the models are used, one where KAN activates itself (grey arrow in plot) and one without this mechanism.

II.v Combining the KAN/REV network with a regulation of miRNAs also results in a model capable of recreating the cell states required for radial patterning

With the KAN interactions in place, the miRNAs can now be added to the system, such that we end up with a network containing both sets of interactions (Figure 14). Because of the increased complexity in the number of species, reactions and variables, no attempt at an analytic solution of this model was made. Instead the equilibrium states of the model are investigated using bifurcation plots (Figure 15).

As for the KAN/REV network, models with and without a KAN self-activating mechanism were investigated. The addition of a KAN self-activating mechanism have a similar effect on the bifurcation plots as it did for the KAN/REV network (cf. Figure 13, 15). However, the difference between networks with/without KAN self-activation was larger when no miRNAs were present. This seems reasonable since a change of the KAN reactions should have a larger impact when only KAN interacts with REV.

Noting that low KAN equilibria corresponds to high REV equilibria, we find that it is hard to get a simultaneously low KAN/REV state. But adding a self-activation to KAN does seem to allow the high REV equilibrium to decrease to about 1/10 of its maximum. This is significant because we want our model to have a gap consisting of cells where both the KAN and REV concentrations are low. These results suggests that a self-activation mechanism makes it easier to sustain simultanously low KAN/REV concentrations despite the negative feedback/switching behaviour.

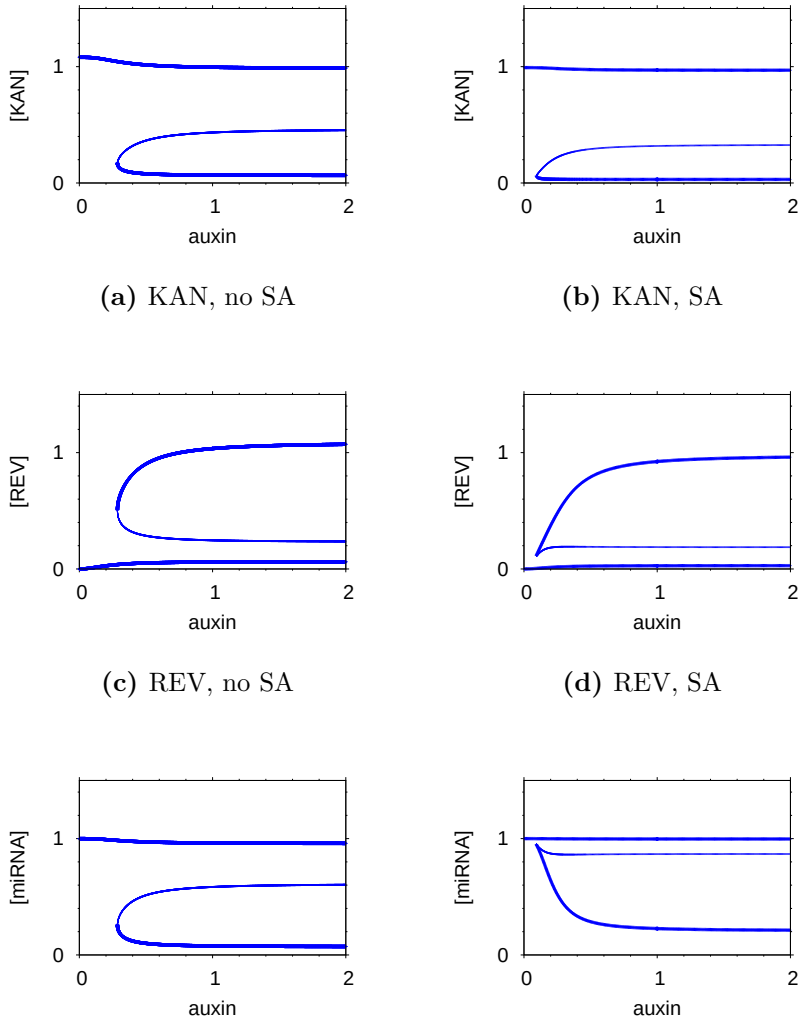

(a) KAN, no SA

(b) KAN, SA

(c) REV, no SA

(d) REV, SA

(e) miRNA, no SA

(f) miRNA, SA

Figure 15: Bifurcation plots with auxin as the parameter for the full model, without KAN self-activation (no SA) and with KAN self-activation (SA). The network is simulated in a single cell; hence there are no signal molecules or diffusion. Low REV concentrations and high KAN/miRNA concentrations belong to the same state, and vice versa. Both networks are seen to be monostable for low levels of auxin, but the monostable region of the no SA network is wider. It is of interest to note that the SA network allows for a better low REV/low KAN/low auxin state.

PC1 important parameters			PC2 important parameters		
V_R (0.54)	K_{2Rr} (0.46)	V_{dRr} (-0.45)	K_{0R} (0.52)	V_{mip} (0.47)	K_{1K} (0.46)

(a) Parameters most important for the PCA, and their weights.

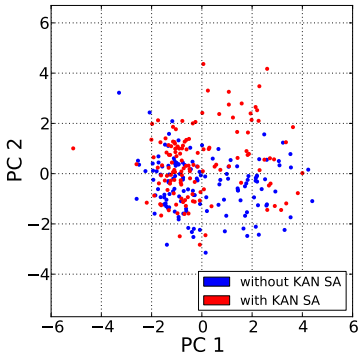

(b) Full model (43%)

Figure 16: Principal component analysis (PCA) of logarithmised parameter sets of the full model with and without KAN self-activation (SA). Each point in the graph represents a set of parameters and the percentage in the parenthesis is the total explained variance by the two components. **(a)** The three parameters with the largest weight (importance) for each principal component (PC) sorted in descending importance. The weights assigned to the components are shown in parenthesis. **(b)** PCA of parameters sets of the full model with and without KAN SA.

II.vi KAN mutants motivates an inhibition of REV by KAN

In previous experiments, it has been found that the SAM continues its activities and that the polarity of leaves survives in KAN loss-of-function (lof) single mutants, while gain-of-function (gof) mutants result in a termination of the SAM and organ initiation [Kerstetter et al., 2001]. In our *in silico* experiments it is seen that the KAN mutants do not alter the expression of any other species in the anchor models (Table 8–10). However this differs from the result of the full models where KAN also acts to inhibit REV. In the full models, the KAN mutants do affect the patterning of the other species, which can be seen in the KAN gof mutants since they destroy the wild type REV and miRNA patterns (Table 11, 3).

The KAN mutants show that the full model has an advantage over the simpler anchor models. Neither of the anchor models were able to create the correct mutant behaviour. A quick inspection of the model reactions reveals that this must be true, since KAN is completely downstream of everything in the anchor models and unable to affect any of the other species. Trivial as this result might then seem, this still provides a motivation for including the additional model interaction where KAN inhibits REV.

II.vii miRNA promoter mutants perturb model species expressions

The existence of regulating miRNAs in the SAM have been inferred indirectly by making changes in the REV mRNA sequence and by observing how the REV expression subsequently increases [Emery et al., 2003]. This proves that REV is downregulated by

something that binds to the REV mRNA, which probably means a miRNA. Incidentally this procedure also creates a REV gof mutant. It is therefore of interest to compare the miRNA lof mutants to the REV gof mutants, and look for similarities and differences. It has also been shown that the KAN gof mutant has a larger impact on the patterning of the meristem than the miRNA gof mutant [Ilegems et al., 2010].

In our models, we assume that the production of miRNAs is facilitated by a promoter. This promoter can be under– or over–expressed in order to create our artificial miRNA mutants.

As expected, the miRNA mutants destroy the patterning when using a miRNA anchor (Table 8) to break the symmetry. It is also found that this model is the only one where the miRNA lof mutant coincide with the expression of the REV gof mutant. In the models with an auxin anchor, the level of REV in the miRNA lof mutant is found to be slightly higher compared to the wild type, but not reaching the levels of the REV gof mutant. This can be argued to still give a qualitatively correct picture.

The miRNA mutants are otherwise seen to alter the patterning of the SAM without destroying it completely (Table 3). Similar to experiments, the miRNA gof function is less fatal to the meristem patterning compared to the KAN gof mutant. In the end, it was decided that a large auxin anchor should be used to set the pattern. These models are only slightly affected by the miRNA mutants, predicting that the miRNAs act to fine-tune the patterning of the meristem.

II.viii REV mutants suggests some additional robustness factor in cells expressing KAN

A decrease in the REV expression leads to plants without axillary meristems and distorted leaves [Talbert et al., 1995]. An increase in REV expression result in radialised vascular tissues, perturbs organ formation and alters leaf morphology [Emery et al., 2003]. In our models, all of the REV mutants extinguishes the patterning of the meristem, except for the lof mutant in the model with large auxin anchor where some of the KAN patterning still is intact (Table 3). It should be noted that experimentally, leaf polarity is not significantly altered by REV gof mutants [Emery et al., 2003]. This contradicts our model predictions where all the gof mutants result in a dominance of REV in the SAM, something which would be expected to impair the formation of organs and destroy their polarity.

The REV mutants can be argued to suggest redundancy among the genes. When the symmetry of the template is broken with a miRNA anchor, the miRNAs sets the *REV* pattern which in turn feedback to the miRNAs. A REV mutant interferes with this loop and therefore destroys the patterning of the template. Similarly, when the symmetry is broken using an auxin anchor activating REV, everything else in the model is thought to follow from the auxin/REV pattern set by the anchor. Therefore it is not surprising that the REV mutants destroy the pattering of the meristem in these models as well. In order to avoid this behaviour and save some of the organ polarity in the REV gof mutants as seen experimentally, some redundancy or additional regulating genes might be needed in order to make the system more robust against these mutant perturbations.

The problem is that when over-expressing REV, cells with high KAN expression should not switch to a REV state. This could also be argued to imply some inherent

robustness in cells with a high KAN expression. Thus, cells with an already high concentration of KAN should be able to resist REV over-expression. For this purpose, the self-activation mechanism for KAN will be investigated more in detail in the next section to see if it can increase the robustness of the model.

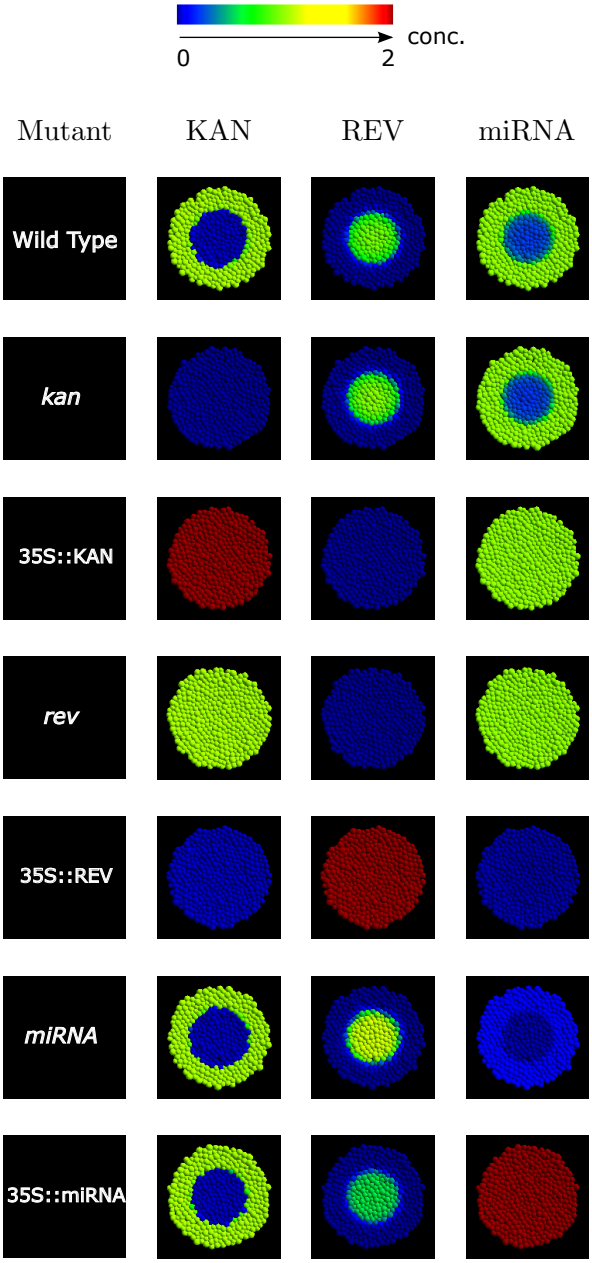

Table 3: Mutant and wild type expression levels for the full model with a KANADI (KAN) self-activation mechanism. Each row corresponds to the mutant specified in the left-most column, and shows the relative expression of the different molecules KAN, REVOLUTA (REV) and miRNA promoter (miRNAp).

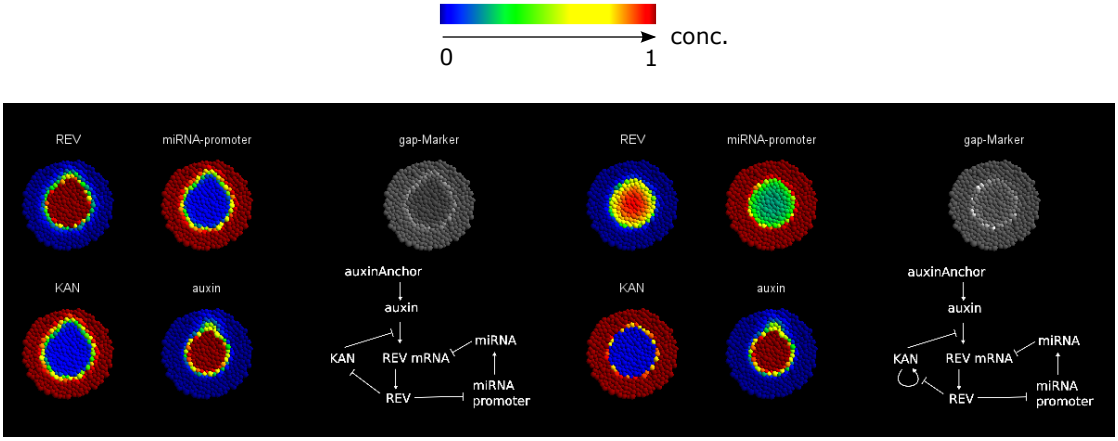

(a) Without self-activation of KAN **(b)** With self-activation of KAN

Figure 17: Models simulated on a template where a peak of auxin has been added at the 12 o'clock position to a meristem in equilibrium. Cell growth was halted while measuring the response to this perturbation. The full model without KAN self-activation showed a clear response where the REV region is distorted upwards and KAN is pushed back where auxin is added, as seen in **(a)**. From **(b)** we can see that the model with a KAN self-activation mechanism seems more robust and the radial symmetry is almost intact despite the perturbed auxin concentrations. It should be noted that the full model without KAN self-activation was shown to be able to create responses similar to **(b)** but without the gap between REV and KAN. The 'gap-Marker' in the plots is designed to be grey in cells with REV or KAN, and white in cells with neither REV or KAN. It is seen that the gap in **(b)** is more white than in **(a)**, indicating that these cells have a lower combined concentration of both KAN and REV.

II.ix KAN self-activation can result in a more robust model and a better gap between KAN and REV

To test our KAN self-activation (SA) hypothesis, we design a simple *in silico* experiment. The system is run on a template with cell growth and cell division until equilibrium is reached and this equilibrium state is then saved. In order to see how the model reacts when adding auxin over the gap between KAN and REV, the saved equilibrium state is modified by adding a peak of auxin in the gap at the 12 o'clock position. Models are then initiated with this new initial state and simulated with cell growth turned off until a new equilibrium has been reached. Cell growth is halted in order to better see how the GRN responds to perturbing the auxin expression, with no cell proliferation complicating the picture.

The model where a self-activation of KAN is included is more robust against an addition of auxin, and has a more distinct gap between KAN and REV (Figure 17) in accordance to unpublished data (private correspondence with M. Heisler). The region with REV is seen to extend further upwards and push back the KAN region considerably in the model with no KAN SA. Also, a better gap with lower concentrations of both REV and KAN was observed in the model with SA, as predicted by the bifurcation analysis.

Note that system behaviour is dependent on the model parameters as well as the

model reactions. Different parameters may result in different outcomes of the experiment, even if the same network is used. To get a more accurate picture several different parameter sets should be used. In addition to the experiments shown here (Figure 17), other parameter sets were also tested. Parameters for which the full model without SA was more robust against auxin perturbations could be found. However, these parameters failed to create a gap with low concentrations of KAN and REV. As a preliminary conclusion, this would mean that both model variants can be robust against auxin perturbation as well as creating a gap between KAN and REV, but only the model with KAN SA can do both.

II.x A relevant auxin distribution in the L1 layer can be created by a PIN1 polarisation transport mechanism together with a central signal

Auxin is thought to be patterned in the meristem using a transport mechanism involving PIN1 proteins. Up to now, the expression of auxin has been set using a static central source of auxin. This sets a constant gradient of auxin throughout the meristem that peaks at the center. However, confocal imaging has shown that a presence of auxin precedes primordia formation. This indicates a dynamic auxin distribution where auxin is transported to sites of primordia initiation. Here we use an auxin transport model where auxin is transported both actively with PIN1 proteins and passively with diffusion [Jönsson et al., 2006]. This model has been shown to be able to generate patterns of varying wavelengths and can establish and maintain inhomogeneous auxin distributions.

The distribution of auxin should fulfil two criteria. First, it should have a static peak in the CZ, such that it sets the central/peripheral identity of the meristem. Second, it should allow for smaller peaks of auxin moving from the CZ to the PZ, marking sites of primordia initiation. A necessary condition for both of these criteria is a model capable of creating inhomogeneous auxin distributions. Therefore the model parameters and underlying auxin source gradient were varied to investigate which parameters/sources that could result in auxin distribution patterns. The total amount of PIN1 in each cell was assumed to be constant and at equal levels in all cells.

It was found that some kind of signal was needed to get a constant peak of auxin in the CZ. A homogeneous source distribution of auxin resulted in floating peaks of auxin, that were randomly distributed. Using the same source gradient as for the auxin anchor model often resulted in sharp small peaks distributed evenly in the CZ, while the PZ was empty. The best results were obtained with a source of auxin that was weighted to have a higher production in the CZ, while having a lower but not insignificant production of auxin in the PZ. For such a distribution of auxin, parameters were found where the CZ was filled with auxin and the PZ contained smaller primordia-marking peaks. In summary, a source gradient of auxin qualitatively similar too, but much smoother, than the previous auxin anchor, was needed to break the symmetry and set the correct auxin distribution.

A mediator molecule X was introduced in order to get the correct dynamics. When the polarisation of PIN1 depended on auxin directly, it was found that peaks of auxin moved from the periphery to the center, while experiments have shown that auxin moves in the other direction; from the center out to the periphery. To remedy this a new

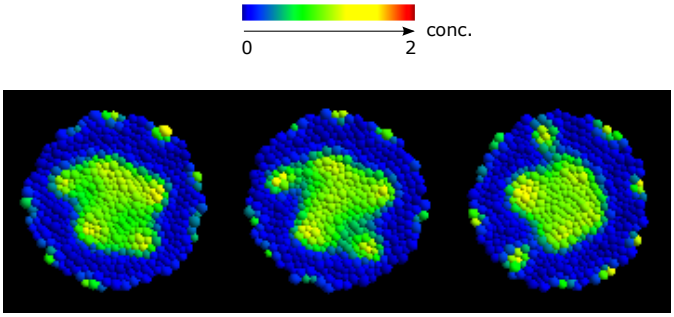

Figure 18: Snapshots of auxin distributions obtained with the PIN1 polarisation transport model. Artifact auxin peaks formed at the outer boundary of the template.

molecule X was introduced to mediate the polarisation of PIN1 by auxin. It was thought that some additional feedback to this molecule X from the network might be required to obtain an appropriate model behaviour. However we begin with the simplest possible hypothesis at our disposal, by creating an X molecule that is linearly activated from auxin, with the same equilibrium concentration, and that plays an identical role as auxin in the polarisation mechanism. This was found to be sufficient to reverse the direction of auxin movement. Thus, adding a linearly activated molecule X results in peaks of auxin being recruited from the CZ to the PZ.

Introducing a mediator effectively creates a lag in the feedback between auxin and PIN1. Also, even though the molecule X is designed to have the same equilibrium concentration as auxin, this concentration might never be reached if it has a slow enough rate of creation/degradation. Note that if X were to reach equilibrium instantly, it would not be expected to alter the model behaviour. The PIN1 polarisation model assumes an instant PIN1 cycling. It could be that this assumption is not valid and that the delay introduced by X would not be needed in a model with a slower PIN1 cycling.

To see if/how the lag introduced by the molecule X affects the transport and distribution of auxin, the combined rate of production/degradation was varied ranging from a slow response to a very fast one. Slow rates of production/degradation resulted in a more fuzzy or blurry pattern of auxin, with a peak in the center and patches of auxin that moved from the center to the periphery. Increasing the rate resulted in somewhat more well-defined patterns but with less movement of auxin from the center to the periphery. By increasing the rate even further a static pattern of auxin was obtained. It might have been expected that a fast enough rate would get us back to the model without the X molecule and reverse the movement of auxin. However this was not observed, instead only static patterns were seen when increasing the production and degradation rate of X.

By including a mediator molecule X with an appropriate rate of creation/degradation to the auxin transport model, and using an asymmetric auxin source gradient, reasonable auxin transport dynamics and distributions could be obtained (Figure 18). The overall qualitative behaviour that was achieved was (i) a large auxin peak in the center and (ii) smaller auxin peaks moving outwards from the center towards the periphery.

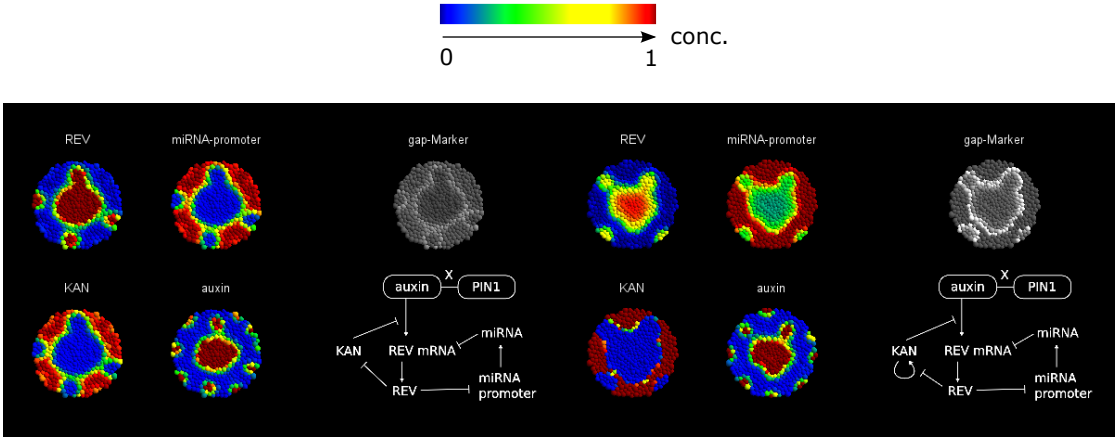

(a) Without self-activation of KAN **(b)** With self-activation of KAN

Figure 19: Snapshots of species concentrations for simulations of the full model interactions including transport of auxin by PIN1 proteins. Four outwards-moving peaks are visible in both **(a)** and **(b)** at varying radii. There are artifact peaks of auxin at the outer boundary of the template, but they are not seen to have a significant effect on the KAN/REV patterning of the meristem.

A minimum rate of cell growth was also needed in order to get dynamic peaks of auxin. It can of course be debated whether the rate of cell growth really should play a key role in the auxin transport model. But the importance of cell growth could perhaps be less significant if other sets of parameters were to be found. Moving peaks of auxin were found in templates without cell growth, but the peaks were either found to move in the wrong direction or unable to define a distinct CZ. It is still conceivable that parameters resulting in the correct behaviour regardless of the rate of cell growth could be obtained with better methods of parameter optimisation.

It should also be noted that unwanted peaks of auxin were seen to form at the outer boundary in the template at constant positions. Changing the size of the template did not remove such boundary peaks. It will be assumed that these peaks are artifacts of the L1 layer model and that they might disappear if a model of the complete SAM were to be used.

II.xi Model predicts central/peripheral patterning in the L1 layer and permits organ initiation

To summarise the results so far, we have a GRN consisting of the antagonistic interactions between KAN/miRNA and REV together with a regulation of REV by miRNAs. We also have a dynamic transport and distribution of auxin by a combination of diffusion and active transport. The GRN has been shown to create the central/peripheral identity of the SAM given an appropriate central signal of auxin. The auxin transport model is seen to create a peak in the center as well as creating smaller peaks moving outwards towards the periphery. Now, we want to add the GRN to the auxin transport model in hopes of obtaining a model allowing for primordia initiation, a central/peripheral

identity of the meristem and an adaxial/abaxial identity of leaf primordia.

The central/peripheral identity of the meristem seemed intact when set by the dynamic auxin distribution (Figure 19). The KAN/REV patterning is only perturbed by the peaks of auxin moving outwards to promote organ formation. The artifact peaks created at the outer boundary of the template does alter this patterning, which could be because they are too shallow to affect *REV*, that they are smoothed out by diffusion or a combination of both. As previously noted, adding a self-activation mechanism to KAN results in a more clear gap between the PZ/CZ. Otherwise, no clear differences between models with/without the self-feedback hypotheses was observed.

As auxin moves into the gap and out towards the periphery, *REV* is turned on while *KAN* and miRNA is turned off. The gap itself does not seem to close; instead a gap is seen to form between every REV/KAN region in simulations with cell growth (Figure 19). Here the mechanism by which the molecules move play an important role. As cells with auxin move radially outwards they stay in their initial high REV/low KAN state. But a cell already in a high KAN state can remain in this state when exposed to auxin (Figure 17). Hence, if KAN moves between cells rather than with the cells, KAN can be allowed to stay on when a primordium-inducing auxin peak move out from the center. Note that in the simulations, KAN is also seen to appear in cells between primordia and the SAM.

Initial behaviour of the model was different from its long-term behaviour. The first peaks of auxin moving had different divergence angles and moved at different rates compared to the peaks of auxin observed at a later time. An exact measurement of the divergence angles was not made, but it was seen that roughly five peaks moved out simultaneously in the beginning. Later, this had changed to a pattern of four peaks at a time. Hence the divergence angles are here seen to decrease with time. As peaks were seen to move out roughly simultaneously, our model would create some kind of whorled phyllotaxis. By tuning the parameters of the underlying auxin transport model, other phyllotactic patterns could perhaps be obtained [Jönsson et al., 2006].

It has been suggested that primordia outgrowth is promoted at the boundary between KAN and REV. In our *in silico* investigation, peaks of auxin is found to spend most of their time in the gap between the CZ and PZ. Once the peaks are disconnected from the CZ they quickly move outwards toward the periphery and subsequently disappears. This temporal asymmetry of auxin can explain why primordia growth is primarily seen in the gap.

III Conclusions and Future Work

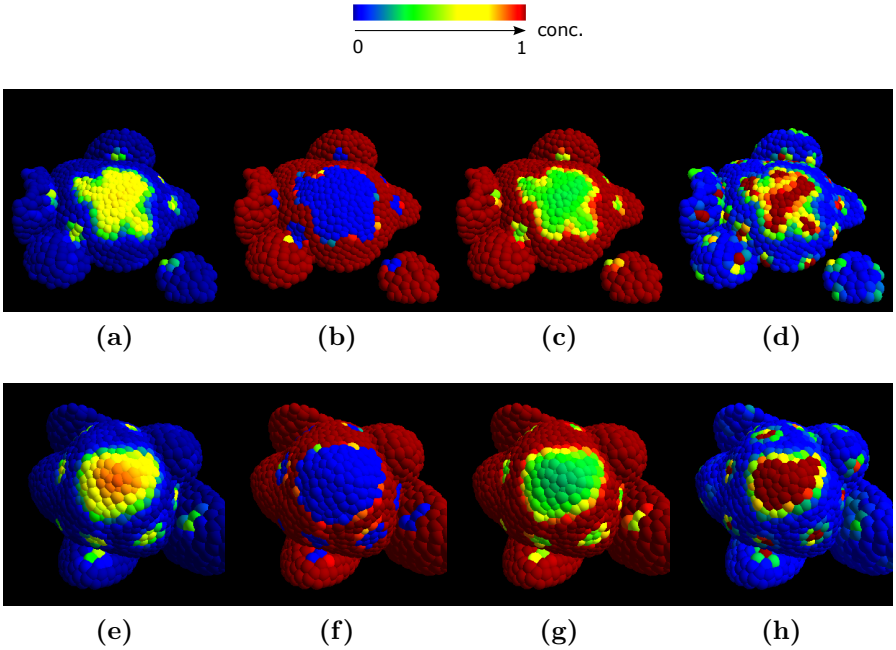

Figure 20: KAN/REV patterning and polarised transport of auxin on cell templates extracted from experimental images. Simulations were carried out on a template of the L1 layer based on data from Caltech and Cambridge. The templates were centred on an auxin signal emanating from the summit of the meristem. The auxin patterning looks noisy but most of this noise does not show up in the KAN/REV expressions. **(a)** REV, **(b)** KAN, **(c)** miRNA promoter, **(d)** auxin concentrations in the Caltech template. **(e)** REV, **(f)** KAN, **(g)** miRNA promoter, **(h)** auxin concentrations in the Cambridge template.

Model predictions include that a central signal is needed in the summit of the meristem to set the auxin distribution and hence the REV expression. Possible origins of this signal can be investigated further. In the current model/parameters no peaks of auxin are created in cells where KAN is already present. Instead auxin moves out with the cells. To test a more realistic primordia initiation in the model, auxin peaks should be created around the gap between KAN and REV. This might be achieved by adding some additional interaction between REV/KAN and auxin/PIN1.

To make the network more robust against REV over-expression, the KAN self-activation mechanism should be investigated into more detail. It is also found that a KAN self-activation mechanism allows genes forming a bistable switch to also have a state with simultaneously low expression of both genes. A KAN self-activation mechanism also might result in a network more resistent to over-expression of REV. Different variants in the formulation of the self-activation could be investigated, e.g., changing the cooperativity of the self-activation might influence the stability and overall behaviour of the network. Different ways KAN and REV interact with the KAN binding site would result in different logics of the KAN promoter activity.

More detailed experimental templates and data will be used to test the model in

a more realistic environment. The model was tested on templates of cells extracted from confocal images (Figure 20). The resulting pattern show some correlation to the positions of developing organs, but since the network is given no information about where the primordium are initiated it cannot fully correlate to the newly formed organs. This model will be used together with templates of more detailed cell structures, including cell walls and non-spherical cells.

A new molecule X was introduced in the signalling pathway between auxin and *PIN1*. The nature of this molecule and the signalling pathway can be investigated further.

IV Methods

IV.i Mathematical modelling

Chemical kinetics

Interactions between genes and their transcripts are modelled either by mass-action or Michaelis-Menten kinetics. In mass-action kinetics the production of a molecule P is proportional to each of the concentrations of the substrates S_i. For example, the reaction

$$S_0 + 2S_1 \underset{k_0}{\longrightarrow} P \underset{k_1}{\longrightarrow} \phi$$

would be governed by the equation

$$\frac{\mathrm{d}[P]}{\mathrm{d}t} = k_0[S_0][S_1]^2 - k_1[P]$$

where brackets denote the concentration of a species. The last term is a degradation term which captures the combined decay of the product P. Note how the production depends on the concentration of S_1 squared, since this molecule occurs twice in the reaction.

In Michaelis-Menten kinetics, the reaction is catalysed by an enzyme E to form an active complex ES

$$E + S \underset{k_1}{\overset{k_0}{\rightleftharpoons}} ES \overset{k_2}{\to} P + E,\ P \underset{k_3}{\longrightarrow} \phi$$

The first set of reactions are assumed to be fast and E, S and ES can be assumed to be at their equilibrium concentrations. The total amount of enzyme E in the cell is assumed to be constant. Hence the reaction rate is limited by the amount of available enzyme as well as the substrate concentration. This reaction is described by

$$\frac{\mathrm{d}[P]}{\mathrm{d}t} = V\frac{[S]^n}{[S]^n + K^n} - k_3[P]$$

The exponent n is related to the number of substrates involved in forming the complex, e.g., if two substrates are needed to form ES, n would be set to two. V sets the maximum value of the production term. When S has the same concentration as the Hill coefficient K, the production term is half of its maximum value.

Modelling of gene regulatory networks

Model species include RNA and proteins. In the case of the modelling of RNA, these are transcribed from DNA, can be downregulated by miRNAs and also has a combined decay rate. As an example, in the final version of the model the concentration [Rr] of the mRNA of REV changes according to

$$\frac{\mathrm{d}[Rr]}{\mathrm{dt}} = \underbrace{V_{Rr}\frac{[A]^2}{K_{0Rr}^2+[A]^2}\frac{K_{1Rr}^2}{K_{1Rr}^2+[K]^2}}_{\text{Transcription}} - \underbrace{V_{dRr}\frac{[mi]^2}{K_{2Rr}^2+[mi]^2}}_{\text{Regulation of miRNAs}} - \underbrace{d_{Rr}[Rr]}_{\text{Decay}}$$

The process of transcription (when RNA is transcribed from DNA), is modelled by Hill functions where the rate of transcription depends on the concentrations of the activators and inhibitor molecules. Activator or inhibitor factors are chained together to form a single Hill function. As a consequence the transcription will always be halted if there is a high concentration of the inhibitor molecule, regardless of the concentration of the activator molecule. Separate Hill functions could also be used for each of the inhibitors and activators. With separate Hill functions the RNA would be transcribed even if there were an high inhibitor concentration, as opposed to our network where an high inhibitor concentration effectively halts transcription.

For the KAN molecule, a small constant basal transcription rate was put into the equation. Due to the self-activation mechanism of KAN, a zero KAN concentration would otherwise completely halt transcription. Without a small basal transcription rate, cells with a zero concentration of KAN would get stuck in this zero state. Cells with high REV/no KAN are supposed to switch to a KAN state when they move to the periphery. The introduction of a basal production rate makes this possible.

miRNAs are assumed to increase the rate of degradation of the messenger RNA [Khanin and Vinciotti, 2008]. This degradation is modelled by a Hill function where miRNA acts as an activator for the degradation. A cooperation of two[1] was assumed for the downregulation of RNA by miRNAs, which makes the degradation more sensitive to the concentration of miRNAs compared to no cooperation.

Translation (when a protein is translated from a RNA) is assumed to be a process that is linear with respect to the RNA concentration. To illustrate this, the concentration of the protein product [R] of *REV* is described by

$$\frac{\mathrm{d}[R]}{\mathrm{dt}} = \underbrace{k_R[Rr]}_{\text{Translation}} + \underbrace{\Delta_R[R]}_{\text{Diffusion}} - \underbrace{d_R[R]}_{\text{Decay}}$$

Diffusion depends on a diffusion constant as well as the concentration gradient of the molecule. The full expression for diffusion of a molecule Y is

$$\Delta_Y[Y] = \sum_{i\in\{\text{neighbours}\}} \delta_Y\Big([Y]-[Y]_i\Big)$$

where δ_Y is the diffusion constant, and sum is carried out on the neighbouring cells of the cell with the concentration Y.

[1]The n of the Hill-function is set to two

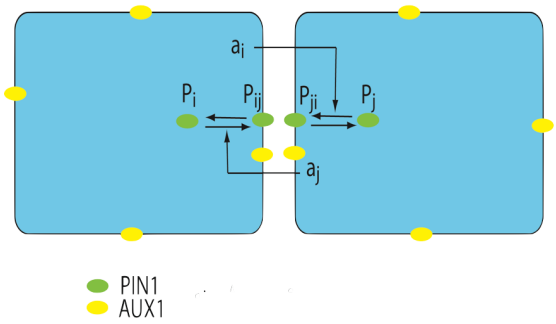

Figure 21: Transport of auxin by polarised PIN1 proteins. Auxin (a_i, a_j) is transported out of the cell by AUX1 and into the cell by PIN1. While AUX1 is assumed to remain at constant concentrations, the PIN1 proteins cycle between the cytosol and the cell membrane. The presence of auxin in neighbouring cells increases the amount of membrane-bound PIN1 proteins.

Modelling auxin transport

It has been shown that a mechanism where auxin influences the polarity of neighbouring auxin efflux/influx mediators is sufficient to create different patterns/distributions of auxin [Jönsson et al., 2006]. In these models of transportation, auxin is assumed to serve as a signal that increases the rate at which PIN1 proteins in neighbouring cells move to the cell membrane (Figure 21). It is assumed that auxin attracts PIN1, such that the concentration of PIN1 is higher in cell membranes facing regions with high levels of auxin. This is how an asymmetric/polarised distribution of PIN1 is created.

The PIN1 molecules cycles between the cytosol and cell membranes. To keep track of the concentrations, $[P_i]$ is used to denote the cytosol concentration of PIN1 in cell i and $[P_{ij}]$ denotes the concentration in the cell membrane of cell i facing cell j. These concentrations change according to

$$\begin{aligned}\frac{\mathrm{d}[P_i]}{\mathrm{d}t} &= -A[P_i]\sum_k a_k + B\sum_k [P_{ik}] \\ \frac{\mathrm{d}[P_{ij}]}{\mathrm{d}t} &= A[P_i][a_j] - B[P_{ij}]\end{aligned}$$

where a_k is the activating signal, i.e., auxin in neighbouring cells. The constants A and B determine the rates of PIN1 cycling to the cell membranes and to the cytosol. The membrane-bound proteins move back into the cytosol at a rate proportional to their concentrations, while the cytosol PIN1 proteins move to the cell membranes at a rate proportional to their concentrations and the concentration of auxin. The PIN1 dynamics are assumed to be fast and we can assume that the proteins concentrations always are at their equilibrium levels,

$$\begin{aligned}P_i &= \frac{(B/A)\,P_{tot}}{\sum_k [a_k] + B/A} \\ P_{ij} &= \frac{[a_j] P_{tot}}{\sum_k [a_k] + B/A}\end{aligned}$$

Rr	*REVOLUTA* mRNA
R	REVOLUTA
K	KANADI
mip	miRNA promoter
mi	miRNA
a	auxin

Table 4: Species of multicellular full model equation.

To obtain these equilibrium concentrations, the total PIN1 concentration P_{tot} in a cell is assumed constant. Brackets are removed from the P's to indicate that these will be treated as parameters (with a value that is determined by the nearby distribution of auxin).

Hence the active polarised transport of auxin between a cell i and its neighbour j is governed by the equation

$$\frac{\mathrm{d}[a_i]}{\mathrm{d}t} = T\left(P_{ji}\frac{[a_j]}{[a_j]+K_a} - P_{ij}\frac{[a_i]}{[a_i]+K_a}\right)$$

where T sets the strength of the active transport and K_a is the Hill coefficient.

In addition to the active transport, auxin is also allowed to diffuse between cells. Taking the production and degradation of auxin into account as well, the total expression for the time dynamics of auxin becomes

$$\frac{\mathrm{d}[a_i]}{\mathrm{d}t} = \underbrace{V_A\frac{R_A^2}{R_A^2+r^2}}_{\text{production}} + \underbrace{T\left(P_{ji}\frac{[a_j]}{[a_j]+K_a} - P_{ij}\frac{[a_i]}{[a_i]+K_a}\right)}_{\text{active transport}} + \underbrace{\Delta\big([a_j]-[a_i]\big)}_{\text{diffusion}} - \underbrace{d_a[a_i]}_{\text{degradation}} \tag{1}$$

Note how the first term breaks the symmetry of the auxin distribution by allowing for a higher production of auxin in cells with a radii $r < R_A$.

Model equations of the full model

The final model contains a negative feedback loop between REV and KAN/miRNA, signal molecules and allows for diffusion (Figure 3). Abbreviations of the molecule names are used to obtain shorter expressions (Table 4).

Note the Hill function in the KAN equation, where the first factor after V_K represents the self-activation of KAN. This factor is not present in the model without self-activation.

The auxin concentration is governed by the PIN1 polarisation transport mechanism (Equation 1).

$$
\begin{aligned}
\frac{\mathrm{d}[Rr]}{\mathrm{dt}} &= V_{Rr}\frac{[a]^2}{K_{0Rr}^2+[a]^2}\frac{K_{1Rr}^2}{K_{1Rr}^2+[K]^2} - V_{dRr}\frac{[mi]^2}{K_{2Rr}^2+[mi]^2} - d_{Rr}[Rr] \\
\frac{\mathrm{d}[R]}{\mathrm{dt}} &= k_R[Rr] + \Delta_R[R] - d_R[R] \\
\frac{\mathrm{d}[K]}{\mathrm{dt}} &= k_K + V_K\frac{[K]^2}{K_{0K}^2+[K]^2}\frac{K_{1K}^2}{K_{1K}^2+[Rr]^2} - d_K[K] \\
\frac{\mathrm{d}[mip]}{\mathrm{dt}} &= V_{mip}\frac{K_{0mip}^2}{K_{0mip}^2+[R]^2} - d_{mip}[mip] \\
\frac{\mathrm{d}[mi]}{\mathrm{dt}} &= k_{mi}[mip] + \Delta_{mi}[mi] - d_{mi}[mi]
\end{aligned}
\tag{2}
$$

IV.ii Simulation software

All model simulations were done with the open software `organism` and visualised with `newman` (both available at `http://dev.thep.lu.se/organism`). The chemical reactions and genetic interactions are defined with `organism` model files, where the set of interactions easily can be modified to test different variants of the reactions. The template of cells in which the reactions occur are defined with `organism` init files. These files contain the coordinates and radii of the cells, as well as initial concentrations. It is possible to use one-, two- or three- dimensional templates with cells. Templates in the form of init files were created either by hand or with Perl scripts.

Cells in our simulations are treated as spheres and are the smallest elements in our templates. Each cell has its own concentrations of the model species. A neighbourhood function is used to continuously find the neighbours of every cell, as the neighbours may change when the cells are growing and dividing. Species may diffuse between neighbouring cells based on the difference in the cell species concentrations.

Cell growth is modelled by an exponential increase of the cell radii [Jönsson et al., 2004,Jönsson et al., 2006,Yadav et al., 2011]. When cells have reached a threshold radius they divide into two new cells with a total combined volume equal to that of their mother cell. The orientation of the new daughter cells are randomly chosen. The mechanics of the system is modelled by springs between the center of the cells. As the cells grow and divide there is a net movement of cell away from the center. Cells outside a threshold distance from the center are removed from the model in order to have a template of constant size.

A fifth order Runge-Kutta solver with an adaptive step-size was used to numerically integrate the ODEs of the system. The result of the integration, i.e., cell positions and cell species concentrations, are saved at different time points, and can be visualised with the software `newman`, specifically developed for this purpose, or any other plotting utility.

IV.iii Analytical solutions and nullclines

Analytical work leading to a formulation of the nullclines was carried out in Sections V.i–V.ii. Dimensionless variables are used, such that focus lies on the qualitative behaviour

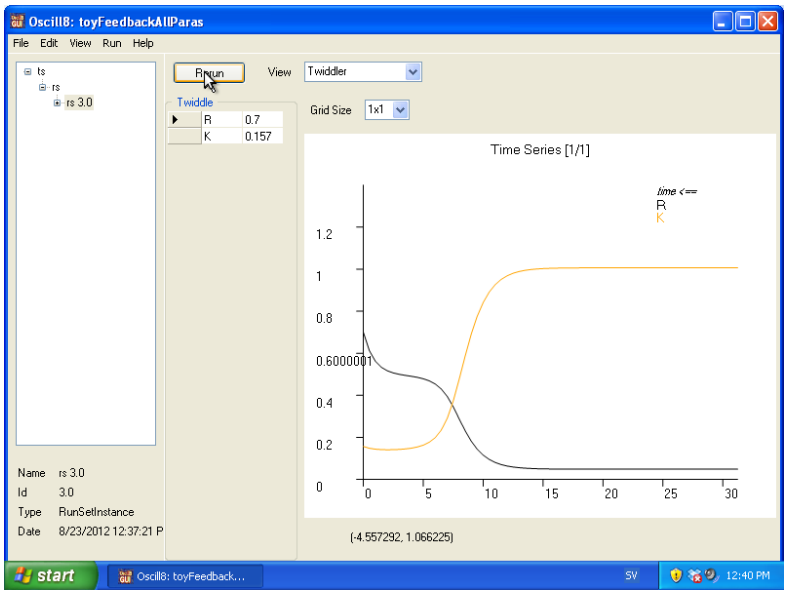

Figure 22: Screenshot of oscill8 running in Windows XP. Windows XP is in turn running under VirtualBox in Ubuntu.

of the network. The dimensionless variables can be converted to the full variables using the results of Section V.ii.

The nullclines of the model were calculated from corresponding analytic expressions. A Perl script was written to calculate the REV/KAN values, stepping through the nullclines with either logarithmic or linear steps. Parameter values determining the shape of the nullclines were allowed to vary within the script. The resulting calculation was visualised with `gnuplot`.

A logarithmic scale was chosen to show the symmetry of the nullclines, while a linear scale was used to make the values of the equilibrium solutions more readable (cf. Figure 12, 25).

IV.iv Bifurcation analysis

The bifurcation analysis was made with the software `oscill8` (Figure 22). Model equations are given to `oscill8` in a .ode file format similar to the one used by the classic `xpp auto` software.

The bifurcation analysis was used to show that the same parameters can have different equilibrium states. To find the different equilibria, several different initial conditions were solved for, revealing all of the possible states that could be reached by the system. These different solutions could then be merged within the software to get the complete bifurcation plot.

Bifurcation data was plotted with `gnuplot` to better be able to customise the plots. Data containing the equilibrium concentrations from different initial conditions were extracted in the `oscill8` raw format, and merged into one file. Data points corresponding to stable fixpoints were separated from the unstable fixpoints and plotted independently in the same plot.

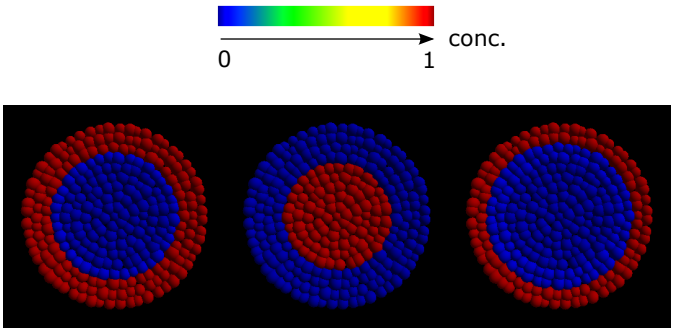

(a) KAN **(b)** REV **(c)** miRNA

Figure 23: The pattern of KAN, REV and miRNA that the models were optimised against. Note that there is a line of cells between the KAN and REV expressions that are empty.

IV.v Parameter optimisations

In the model equations (e.g., Equations 2, 1) parameter values need to be set for the various reactions. No values were taken from experimental data, instead parameter values were found by fitting the model to a predefined pattern. How close the model is to recreate the pattern is defined either by a cost function or, when finding parameters for the auxin transport model, by inspection of the equilibrium state.

Optimising against the KAN, REV and miRNA patterns

A circular static template with 279 cells was used in the parameter optimisations. To find parameters recreating a certain pattern, we first need to define the pattern in the reference template. This template is designed to have idealised binary concentrations of the species. Here, we optimise with respect to REV, KAN and miRNA (promoter activity) expressions (Figure 23). Random values between zero and one are used as initial values of the parameters.

The optimisation algorithm is a biased random search based on a system of tokens that rewards steps in succesful directions in parameter space [Gruel et al., 2009]. Each parameter and direction is initialised with an equal amount of tokens. The probability of varying a parameter in a certain direction is proportional to the number of token this direction has. This means that initially, each direction in parameter space is equally probable.

After a direction in parameter space has been choosen, the system is integrated until an equilibrium has been reached. Equilibrium is said to occur when the squared-sum difference between the species concentrations of the current state and the state at the previous time point falls below a set threshold. When equilibrium is reached, the state is compared to the reference template. An energy function defined as the squared-sum difference between the reference template concentrations c^* and the equilibrium concentrations c is used to measure how close the state is to the reference,

$$E = \sum_{\text{species}(i)} \sum_{\text{cells}(j)} \left(c_{ij} - c^*_{ij}\right)^2$$

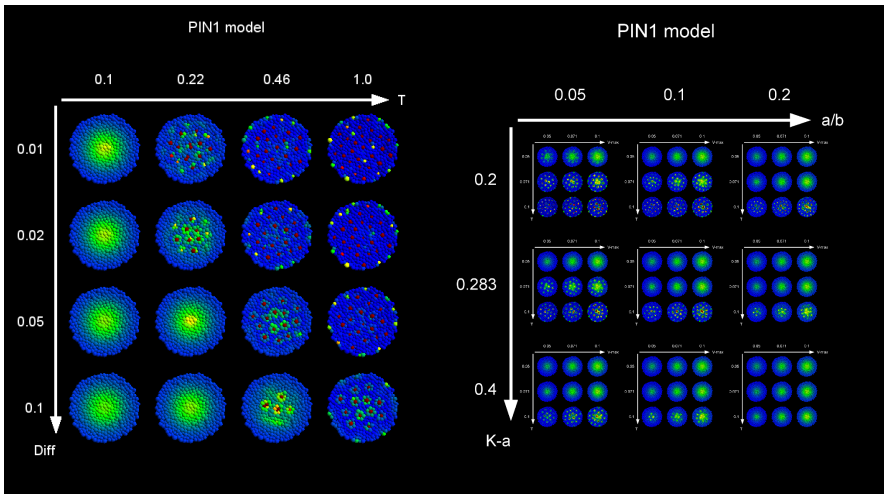

(a) Variation of 2 parameters **(b)** Variation of 4 parameters

Figure 24: Example of an optimisation of the PIN1 model. **(a)** A snapshot of the auxin distribution for different values of the diffusion constant **Diff** and the active transport constant **T**. Templates in the same diagonal look similar to each other and have the same **T**/**Diff** ratio in. This indicates that only the ratio between active and passive transport is important for the patterning generating abilities of the model. Note that numbers in the axes have been rounded differently. **(b)** Example of a plot where four parameters have been varied.

where c_{ij} is the concentration of species i in cell j.

If a step in the parameter space result in a better equilibrium state, this direction is rewarded with an additional token, if there are any left in the pool of free tokens. If a step results in a worse equilibrium state, this direction has one token removed and put into the pool of free tokens. Then a new step is made where the direction is chosen with the new updated probabilites.

Each optimisation run consisted of 3000 steps, and optimisations were run until about 100 good parameter sets had been found. A parameter set was considered to be good if the calculated energy was below a threshold value.

Optimising parameters for the auxin distribution

When finding parameters for the model of the auxin transport, a dynamic circular template of cells with cell growth and cell division was used. A pattern of a large central auxin peak and smaller auxin peaks moving from the center to the periphery was sought. Because of the movement of cells resulting from the cell growth, it becomes hard to follow the positions of the cells in the template, making it troublesome to define a proper energy function. Also, the distribution of auxin is assumed to be dynamic, further complicating the design of an energy function, as the auxin distribution would have to be compared to several snap-shots of auxin distributions at different time points.

For the above reasons, the previous described optimisation algorithm did not work when optimising the auxin transport model. The problem lies in comparing a dynamic auxin distribution from a simulation to a reference distribution. However, for a human

eye, a quick glance at an auxin distribution is enough to tell if it is a good or a bad one.

With this in mind a script was written in python, which scans the parameter space of the model. A snapshot of the equilibrium distribution is saved for each scanned point in the parameter space. This snapshot can then be plotted on a grid with the parameter values of the model (Figure 24). This gives us an idea of how the patterning capabilities of the model relates to its parameters, as well as allowing us to find the good parameters of the model.

When searching for a specific auxin distribution, four model parameters were varied at a time in order to span a large region in parameter space but with low resolution. From this rough overview, regions with some patterning capabilites can be found. These regions can in turn be scanned more in depth, to investigate a smaller region in the parameter space but with a higher resolution. After several iterations of this process, good pattern-generating parameters were eventually found.

IV.vi Sensitivity analysis

Sensitivity analysis provides a measure of the robustness of a model. The following discrete expression for the sensitivity s when varying parameter p was used,

$$s = \frac{\Delta c/c}{\Delta p/p} \tag{3}$$

This is a measure of how much a fractional change in a parameter perturbs a concentration c, relative to the concentrations of a default template. A sensitivity of one means that the system responds to a one percent increase of a parameter with a one percent increase in the concentration. This would be a response that is linear with respect to that parameter. Sensitivity less than one indicates robustness and the presence of some dampening feedback while sensitivity over one indicates the presence of instabilities.

The full expression used for calculation of the sensitivy s_{ij} of species i and parameter p_j was

$$s_{ij} = \frac{1}{n} \sum_{\text{parasets}} \frac{p_j}{\Delta p_j} \sum_{\text{cells}} \frac{c^*_{ij} - c_i}{c_i}$$

where c^*_{ij} is the perturbed concentration of species i when varying parameter j and c_i is the original template concentration. The sum is carried out on all the cells in a template, and for n different sets of parameters (parasets). Each parameter was varied with one percent, meaning that $p_j/\Delta p_j = 100$ for all j. This was done for 120 ($\pm$ 10) sets of parameters for each of the models.

The sign of the sensitivity can tell us in which direction the expression is perturbed. This method of calculating the sensitivity might skew the result if one half of the cells were to change concentrations in one direction and the other half were to change their concentrations in the other direction. In this case, the perturbations would cancel and a very small sensitivity would result, regardless of how large the variation would be. But this should not pose a problem since e.g., a parameter that determines the production of a species should change the production in the same direction in every cell. It should however be noted that the validity of the sensitivity analysis relies on the assumption

that a change in a parameter perturbs all cell concentrations of a species in the same direction.

The sensitivity analysis was carried out with a Perl script modified to allow for a calculation of means and variances of sensitivities for several parameter sets and customised for three different species.

IV.vii Principal component analysis

The PCA was carried out using the Modular toolkit for Data Processing (MDP) [Zito et al., 2008] in Python and visualised with the module `matplotlib`. Additional statistics, such as the weights for the principal components, were obtained from a PCA done with `Project R`. Thus two different pieces of software were used for the PCA; MDP was used for better and more customisable plots while the `Project R` software was used for more detailed statistics. The PCA plots for both softwares were also compared and seen to give consistent results.

Parameters were preprocessed for the PCA by logarithmising and then normalising the parameters to zero mean and unit variance. The normalisation of logarithmised parameters $\log(p)$ to zero mean is equivalent to normalising the parameters p to have a unit geometrical mean. This follows from the definition of the mean

$$\begin{aligned} 0 = E &= \frac{1}{n}\sum_i^n \log p_i \\ &= \frac{1}{n}\log\left[\prod_i^n p_i\right] \\ &= \log\left[\left(\prod_i^n p_i\right)^{1/n}\right] \end{aligned}$$

By taking the exponent of both sides we get

$$1 = \left(\prod_i^n p_i\right)^{1/n}$$

where the right hand side can be recognised as the geometric mean. Hence the parameters are effectively normalised to unit geometric mean.

When comparing parameter sets between different models in a PCA, some parameters are not present in all models. These parameters are discarded from the analysis. Instead, if the models contain parameters with similar function and have the same name, these parameters are merged and exposed to the same PCA. For example, there were some overlap in parameters between the models with an auxin anchor and a miRNA anchor (Figure 7), therefore these were analysed in the same PCA. The plotting was done using `pyplot`.

IV.viii Mutants

Mutants are created by modifying the production rate of the molecules. The result is either an over-expression or an under-expression of the molecule, compared to the wild type expression.

Mutants under-expressing a molecule were made by reducing all production terms of the corresponding molecules with a factor ten. Mutants over-expressing a species (35::S mutants) were created by adding an equal production of the molecule in every cell set at twice the total wild type production rate.

V Appendix

V.i Analytical solution of the KAN/REV sub network

In order to get a better understanding of the system, the simplified KAN/REV network (Figure 11) was solved analytically. From a modelling perspective, the auxin anchor variable can be seen as a control parameter which we want to use to toggle between different possible equilibrium states of the system. Hence it is of interest to see how the equilibrium solution depends on both the parameters and the level of auxin.

To solve the system, equilibrium is assumed by setting the time derivates of the model equations (Equations 11) to zero,

$$\begin{aligned}
0 &= V_R \frac{[A]^{n_{0R}}}{K_{0R}^{n_{0R}} + [A]^{n_{0R}}} \frac{K_{1R}^{n_{1R}}}{K_{1R}^{n_{1R}} + [K]^{n_{1R}}} - d_R[R] \\
0 &= V_K \frac{[K]^{n_{0K}}}{K_{0K}^{n_{0K}} + [K]^{n_{0K}}} \frac{K_{1K}^{n_{1K}}}{K_{1K}^{n_{1K}} + [R]^{n_{1K}}} - d_K[K] \\
0 &= k_A[aA] - d_A[A]
\end{aligned}$$

We will work under the assumption that all n's are two in order to reduce the number of free parameters. We can also set $k_A = d_A$, and instead tune the constants in the [A] factor of the first equation, or change the value of the auxin anchor. With this in mind we get

$$\begin{aligned}
0 &= V_R \frac{[aA]^2}{K_{0R}^2 + [aA]^2} \frac{K_{1R}^2}{K_{1R}^2 + [K]^2} - d_R[R] \\
0 &= V_K \frac{[K]^2}{K_{0K}^2 + [K]^2} \frac{K_{1K}^2}{K_{1K}^2 + [R]^2} - d_K[K]
\end{aligned}$$

if we exchange $[A]$ for $[aA]$.

The first factor containing the auxin concentration can be treated as one parameter to further simplify things. Define an effective V_R^* that depends on the level of auxin,

$$V_R^* = V_R^*([aA]) = V_R \frac{[aA]^2}{K_{0R}^2 + [aA]^2}$$

The system of equations now looks like

$$\begin{aligned}
0 &= V_R^* \frac{K_{1R}^2}{K_{1R}^2 + [K]^2} - d_R[R] \\
0 &= V_K \frac{[K]^2}{K_{0K}^2 + [K]^2} \frac{K_{1K}^2}{K_{1K}^2 + [R]^2} - d_K[K]
\end{aligned}$$

We can divide these equations with any value without changing the equilibrium solutions. Use this fact to divide each equation with its degradation term in order to remove these three parameters from the system. Then define new reduced parameters as

$$\cancel{A}_i = \frac{A_i}{d_i}$$

We then get an equation system that reads

$$\begin{aligned} 0 &= \cancel{V}_R^* \frac{K_{1R}^2}{K_{1R}^2 + [K]^2} - [R] \\ 0 &= \cancel{V}_K \frac{[K]^2}{K_{0K}^2 + [K]^2} \frac{K_{1K}^2}{K_{1K}^2 + [R]^2} - [K] \end{aligned} \tag{4}$$

It is possible to further reduce the number of parameters in this equation by making appropriate variable substitutions. However, there is a point in keeping the K's of the Hill functions. The K and V parameters both have a clear interpretation, while the dimensionless quantities that you would obtain from a variable substitution often do not.

Without auxin

When we do not have any auxin, $\cancel{V}_R^* = 0$ in Equation (4), and we obtain

$$\begin{aligned} 0 &= [R] \\ 0 &= [K] \left(\cancel{V}_K \frac{[K]}{K_{0K}^2 + [K]^2} - 1 \right) \end{aligned}$$

which have a trivial solution in

$$\begin{aligned} [R] &= 0 \\ [K] &= 0 \end{aligned}$$

Looking into the case where $[K] \neq 0$ we get the equations

$$\begin{aligned} 0 &= [R] \\ 0 &= [K]^2 - \cancel{V}_K [K] + K_{0K}^2 \end{aligned}$$

with the solutions

$$\begin{aligned} [R] &= 0 \\ [K] &= \frac{\cancel{V}_K}{2} \pm \sqrt{\left(\frac{\cancel{V}_K}{2} \right)^2 - K_{0K}^2} \end{aligned}$$

Note that this expression only depends on the parameters $\cancel{V}_K$ and K_{0K}. This can be explained by noticing that an absence of auxin implies that the REV concentration is always zero, hence all REV-related parameters cancels or disappears from the solution.

In the no auxin case we thus have three possible solutions which typically corresponds to two stable fixpoints. However, it is not possible to know which of the fixpoints that are stable and which is unstable from just looking at the solutions.

With auxin

Beginning with Equations (4), the last equation can be reformulated to yield

$$0 = \cancel{V}_R^* \frac{K_{1R}^2}{K_{1R}^2 + [K]^2} - [R]$$
$$0 = [K]\left(K_{0K}^2 + [K]^2 - \cancel{V}_K \frac{K_{1K}^2}{K_{1K}^2 + [R]^2}[K]\right)$$

and we see that one solution to the system is

$$[R] = \cancel{V}_R^*$$
$$[K] = 0 \tag{5}$$

The other solution(s) are given by solving the second order equation

$$0 = [K]^2 - \cancel{V}_K \frac{K_{1K}^2}{K_{1K}^2 + [R]^2}[K] + K_{0K}^2$$

which can be solved for [K] to obtain

$$[R] = \cancel{V}_R^* \frac{K_{1R}^2}{K_{1R}^2 + [K]^2}$$
$$[K] = \cancel{V}_K \frac{K_{1K}^2}{2\left(K_{1K}^2 + [R]^2\right)} \pm \sqrt{\left(\cancel{V}_K \frac{K_{1K}^2}{2\left(K_{1K}^2 + [R]^2\right)}\right)^2 - K_{0K}^2} \tag{6}$$

These non-linear equations are still coupled. Variable substitutions could be made but that would only result in very messy expressions. It is hard to imagine that further insight would be achieved from such a variable substitution. Instead we solve this system graphically/numerically (Figure 12–13). Finally, it should be noted that both of the above solutions reduce to the no auxin solutions by setting $\cancel{V}_R^* = [R] = 0$. Hence solutions 5–6 also includes the result from the previous section.

V.ii Relationship between networks with/without a KAN self-activation mechanism

Remembering the model equations for the KAN/REV network (Equations 11), we see that the self-activation factor becomes unity and disappears if we set $K_{0K}^{n_{0K}} = 0$. This is only valid together with the assumption that $[K] \neq 0$. Setting $K_{0K}^{n_{0K}} = 0$ and $[K] \neq 0$ thus reduces the network with self-activation to the network without self-activation.

This can be exploited to see how the equilibrium solutions change due to the self-activation mechanism. Solution (5) is rendered moot since we require that $[K] \neq 0$. However, solution (6) becomes

$$[R] = \cancel{V}_R^* \frac{K_{1R}^2}{K_{1R}^2 + [K]^2}$$
$$[K] = \cancel{V}_K \frac{K_{1K}^2}{2\left(K_{1K}^2 + [R]^2\right)} \pm \cancel{V}_K \frac{K_{1K}^2}{2\left(K_{1K}^2 + [R]^2\right)}$$

Again, we cannot have $[K] = 0$, so we are left with

$$[R] = \cancel{V_R^*} \frac{K_{1R}^2}{K_{1R}^2 + [K]^2}$$
$$[K] = \cancel{V_K} \frac{K_{1K}^2}{K_{1K}^2 + [R]^2} \tag{7}$$

We can transform this into dimensionless variables to easier see the overall qualitative behaviour. Begin by defining

$$r = \frac{[R]}{K_{1K}}$$
$$k = \frac{[K]}{K_{1R}}$$

which leads to solutions that takes the form

$$r = \frac{\cancel{V_R^*}}{K_{1K}} \frac{1}{1 + k^2}$$
$$k = \frac{\cancel{V_K}}{K_{1R}} \frac{1}{1 + r^2}$$

if we further define

$$\alpha = \frac{\cancel{V_R^*}}{K_{1K}}$$
$$\beta = \frac{\cancel{V_K}}{K_{1R}}$$

the solutions are given by

$$r = \frac{\alpha}{1 + k^2}$$
$$k = \frac{\beta}{1 + r^2}$$

Genetic networks with solutions of these forms have been investigated and have been shown to exhibit bistability for certain parameter regions (Gardner et.al., 2000). Our model with a self-activation mechanism can be seen as an extension of these genetic networks.

The total number of parameters defining the system has now been reduced from six to two. This should not come as a surprise, since it is shown in Section V.iii is is possible to reduce the number of parameters by twice the number of species. Here, we have two species and begin with six parameters (counting V_R^* as a single parameter), which means that it is possible to reduce the number of parameters to two.

Using the same definitions as above, the solutions (6) for the network with KAN self-activation becomes

$$r = \frac{\alpha}{1 + k^2}$$
$$k = \frac{\beta}{2(1 + r^2)} \pm \sqrt{\left(\frac{\beta}{2(1 + r^2)}\right)^2 - \gamma^2}$$

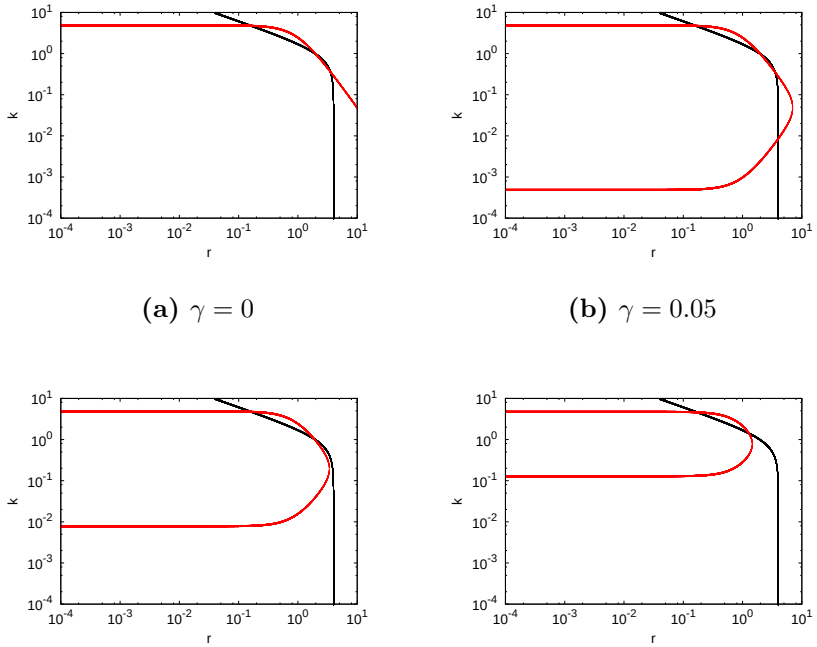

(a) $\gamma = 0$ **(b)** $\gamma = 0.05$

(c) $\gamma = 0.2$ **(d)** $\gamma = 0.8$

Figure 25: r, k nullclines in log space for different values of γ. Otherwise the parameters are set to $\alpha = 4$ and $\beta = 5$. When γ is zero, we get the nullclines of a model without self-activation. Increasing γ results in two solutions for which the maximum moves toward lower values of r for higher values of γ. In addition to the nullclines shown, we also have the nullcline k = 0 (impossible to show here because of the log scale). Further take note of how the number of fix points differ between different values of γ.

with the additional constant

$$\gamma = \frac{K_{0K}}{K_{1R}}$$

With these new dimensionless parameters, the self-activaton of KAN disappears if we take $\gamma = 0$ and keep the positive square root term. Here, $\gamma = 0$ corresponds to setting $K_{0K} = 0$ and keeping the positive square root term corresponds to discarding the $[K] = 0$ solution. Both of these assumptions were previously shown to reduce the network with KAN self-activation to a network without the self-activation mechanism.

Note that these two assumptions are interdependent. If we take $\gamma = 0$ we also must have that $[K] \neq 0$ in order to avoid an illdefined $0/0$ expression in the model equations. On the other hand, if we take $\gamma \neq 0$, $[K]$ can in principle take on any value allowed by the model parameters, including zero.

One difference between the models is therefore the possibility of a solution with $[K] = 0$ in the self-activation network. In effect, the KAN self-activation mechanism splits the KAN nullcline into two separate ones, one at high levels of KAN, and one at lower levels of KAN. Increasing γ shifts the lower KAN nullcline upwards, and shifts the upper KAN nullcline downwards (Figure 25).

V.iii Reducing the number of parameters in a biological system

In order to explain and get an idea of how far it is possible to reduce the number of parameters in a system of ODEs, an attempt to derive how far it is possible to reduce the number of parameters is made.

Assume we have a system of ODEs with $n+1$ species, where the time derivative of each species depends on a total of m_n parameters. Give every parameter an unique index such that the first parameter of the first species is called p_0, the last parameter of the first species is called p_{m_0}, the first parameter of the second species is called p_{m_0+1}, and so on. Then we can write

$$\begin{aligned}
\frac{\mathrm{d}[X_0]}{\mathrm{dt}} &= f_0\Big([X_0],[X_1],\ldots,[X_n]\,;\,\mathrm{p}_0,\mathrm{p}_1,\ldots,\mathrm{p}_{m_0}\Big)\\
\frac{\mathrm{d}[X_1]}{\mathrm{dt}} &= f_1\Big([X_0],[X_1],\ldots,[X_n]\,;\,\mathrm{p}_{m_0+1},\mathrm{p}_{m_0+2},\ldots,\mathrm{p}_{m_1}\Big)\\
&\vdots \qquad \vdots\\
\frac{\mathrm{d}[X_n]}{\mathrm{dt}} &= f_n\Big([X_0],[X_1],\ldots,[X_n]\,;\,\mathrm{p}_{m_{(n-1)}+1},\mathrm{p}_{m_{(n-1)}+1},\ldots,\mathrm{p}_{m_n}\Big)
\end{aligned}$$

We are mainly interested in the equilibrium solutions of a system. In equilibrium, all time derivatives are zero and we get

$$\begin{aligned}
0 &= f_0\Big([X_0],[X_1],\ldots,[X_n]\,;\,\mathrm{p}_0,\mathrm{p}_1,\ldots,\mathrm{p}_{m_0}\Big)\\
0 &= f_1\Big([X_0],[X_1],\ldots,[X_n]\,;\,\mathrm{p}_{m_0+1},\mathrm{p}_{m_0+2},\ldots,\mathrm{p}_{m_1}\Big)\\
&\vdots \quad \vdots\\
0 &= f_n\Big([X_0],[X_1],\ldots,[X_n]\,;\,\mathrm{p}_{m_{(n-1)}+1},\mathrm{p}_{m_{(n-1)}+2},\ldots,\mathrm{p}_{m_n}\Big)
\end{aligned}$$

Now note that we may rewrite any Hill function along the lines

$$\begin{aligned}
\mathrm{H}_0\Big([X]\Big) &= V\,\frac{K^\alpha}{K^\alpha+[X]^\alpha}\\
&= V\,\frac{1}{1+\left(\frac{[X]}{K}\right)^\alpha}
\end{aligned}$$

and make a variable substitution to dimensionless parameters as in

$$\begin{aligned}
x &= \frac{[X]}{K}\\
&\Updownarrow\\
[X] &= Kx
\end{aligned}$$

These kinds of variable substitutions can be used to remove up to one parameter for each ODE. If the ODE does not contain a Hill function, it probably contains some term of the form $f_{\mathrm{term}}\big([X]\big) = k\cdot[X]^\alpha$ instead, where k and α are real positive numbers, and a similar reduction of the number of parameters by a variable substitution can be achieved.

However, one might be concerned that although the substitution $x = [X]/K$ removes one parameter for one term, it may also have the undesirable side effect of introducing the K somewhere else. This, although true, can be properly accommodated for in the following way.

Assume we have transformed our variable as $[X] = a \cdot x$. If the variable [X] would appear in a Hill function, it is always possible to rescale the K's of that Hill function in the opposite direction in order to compensate for the change of variables. Let H_1 be a Hill function that depends on the old variable $[X]$. We would then rescale the K's to new $\overline{K}$'s as

$$\begin{aligned}
\mathrm{H}_1\Big([X] = a\,x\Big) &= V\,\frac{K^\alpha}{K^\alpha + [X]^\alpha} \\
&= V\,\frac{K^\alpha}{K^\alpha + (a\,x)^\alpha} \\
&= V\,\frac{\left(\frac{K}{a}\right)^\alpha}{\left(\frac{K}{a}\right)^\alpha + x^\alpha} \\
&= V\,\frac{(\overline{K})^\alpha}{(\overline{K})^\alpha + x^\alpha}
\end{aligned}$$

This concept can be applied to all Hill functions, and every term of the form $f_{\mathrm{term}}\big([X]\big) = k \cdot [X]^\alpha$. Since chemical reactions that follow the law of mass action results in terms of the latter form, and Michaelis–Menten kinetics is described by Hill functions, we would expect that almost every term in a biological system of ODEs can be properly rescaled to compensate for any change of variables.

The net effect of making the variable substitutions to new x_i variables is a reduction of one parameter per species, for a total reduction of n parameters, and the introduction of new $\overline{\mathrm{p}}_{\overline{m}_j}$ parameters with updated indices.

Now assume that we have done the variable substitution in this way. We end up with a system of equations with n less parameters, that reads

$$\begin{aligned}
0 &= f_0\Big(x_0, x_1, \ldots, x_n\,;\, \overline{\mathrm{p}}_0, \overline{\mathrm{p}}_1, \ldots, \overline{\mathrm{p}}_{\overline{m}_0}\Big) \\
0 &= f_1\Big(x_0, x_1, \ldots, x_n\,;\, \overline{\mathrm{p}}_{\overline{m}_0+1}, \overline{\mathrm{p}}_{\overline{m}_0+2}, \ldots, \overline{\mathrm{p}}_{\overline{m}_1}\Big) \\
&\;\;\vdots \quad\;\; \vdots \\
0 &= f_n\Big(x_0, x_1, \ldots, x_n\,;\, \overline{\mathrm{p}}_{\overline{m}_{(n-1)}+1}, \overline{\mathrm{p}}_{\overline{m}_{(n-1)}+2}, \ldots, \overline{\mathrm{p}}_{\overline{m}_n}\Big)
\end{aligned}$$

where $\overline{\mathrm{p}}_{\overline{m}_k}$ is the last parameter of the kth species.

It is possible to further reduce the number of constants. One property of this system of equations is that we can multiply each equation with any factor and still get the same equilibrium solutions. In general this means that we can use this to divide each equation with a parameter, usually a rate constant, such that we remove this parameter from the equation. If we do this for each equation we further reduce the number of parameters

by n and get a system of ODEs with new parameters and new indices,

$$
\begin{aligned}
0 &= f_0\Big(x_0, x_1, \ldots, x_n \,;\, \text{\reflectbox{R}}_0, \text{\reflectbox{R}}_1, \ldots, \text{\reflectbox{R}}_{\overline{\overline{m}}_0}\Big) \\
0 &= f_1\Big(x_0, x_1, \ldots, x_n \,;\, \text{\reflectbox{R}}_{\overline{\overline{m}}_0+1}, \text{\reflectbox{R}}_{\overline{\overline{m}}_0+2}, \ldots, \text{\reflectbox{R}}_{\overline{\overline{m}}_1}\Big) \\
&\vdots \quad \vdots \\
0 &= f_n\Big(x_0, x_1, \ldots, x_n \,;\, \text{\reflectbox{R}}_{\overline{\overline{m}}_{(n-1)}+1}, \text{\reflectbox{R}}_{\overline{\overline{m}}_{(n-1)}+2}, \ldots, \text{\reflectbox{R}}_{\overline{\overline{m}}_n}\Big)
\end{aligned}
$$

Note that the new parameters $\text{\reflectbox{R}}_0, \ldots, \text{\reflectbox{R}}_{\overline{\overline{m}}_n}$ are all functions of the old parameters $p_0, \ldots, p_{m_n}$.

In conclusion, in a system of n species, it is possible to reduce the number of parameters by $2n$ in a system of ODEs describing mass action and Michaelis–Menten kinetics, by means of variable substitution and by multiplying each equation with appropriate factors.

Rr	REVOLUTA mRNA
R	*REVOLUTA*
K	*KANADI*
mi	miRNA
mip	miRNA promoter
A	auxin
miA	miRNA anchor

Table 5: Legend for miRNA anchor and auxin anchor model equations.

V.iv Equations of the anchor models

In the miRNA anchor model, the outermost cells contain an anchor molecule which functions as a constant source of miRNAs.

For the auxin anchor models, the anchor term in the auxin equation sets a production rate that depends on the distance from the center of the template. Cells inside a certain radius, $r < R_A$, will have a production of auxin.

Equations describe the dynamics of KAN, REV, miRNA and/or auxin (Table 5).

miRNA anchor model

$$\begin{aligned}
\frac{\mathrm{d}[Rr]}{\mathrm{dt}} &= k_{Rr} - V_{dRr}\frac{[mi]^2}{K_{2Rr}^2 + [mi]^2} - d_{Rr}[Rr] \\
\frac{\mathrm{d}[R]}{\mathrm{dt}} &= k_R[Rr] - d_R[R] \\
\frac{\mathrm{d}[K]}{\mathrm{dt}} &= V_K\frac{K_{1K}^2}{K_{1K}^2 + [R]^2} - d_K[K] \\
\frac{\mathrm{d}[miA]}{\mathrm{dt}} &= 0 \\
\frac{\mathrm{d}[mip]}{\mathrm{dt}} &= k_{mip}[miA] + V_{mip}\frac{K_{0mip}^2}{K_{0mip}^2 + [R]^2} - d_{mip}[mip] \\
\frac{\mathrm{d}[mi]}{\mathrm{dt}} &= k_{mi}[mip] + \Delta_{mi}[mi] - d_{mi}[mi]
\end{aligned} \tag{8}$$

Auxin anchor model

$$
\begin{aligned}
\frac{\mathrm{d}[A]}{\mathrm{dt}} &= \mathrm{anchor}(r) + \Delta_A[A] - d_A[A] \\
\frac{\mathrm{d}[Rr]}{\mathrm{dt}} &= k_{Rr}[A] - V_{dRr}\frac{[mi]^2}{K_{2Rr}^2 + [mi]^2} - d_{Rr}[Rr] \\
\frac{\mathrm{d}[R]}{\mathrm{dt}} &= k_R[Rr] - d_R[R] \\
\frac{\mathrm{d}[K]}{\mathrm{dt}} &= V_K\frac{K_{1K}^2}{K_{1K}^2 + [R]^2} - d_K[K] \\
\frac{\mathrm{d}[mip]}{\mathrm{dt}} &= V_{mip}\frac{K_{0mip}^2}{K_{0mip}^2 + [R]^2} - d_{mip}[mip] \\
\frac{\mathrm{d}[mi]}{\mathrm{dt}} &= k_{mi}[mip] + \Delta_{mi}[mi] - d_{mi}[mi]
\end{aligned} \tag{9}
$$

The anchor term is defined as

$$
\mathrm{anchor}(r) = V_A\frac{R_A^{20}}{R_A^{20} + r^{20}}
$$

R	REVOLUTA
K	KANADI
A	auxin
aA	auxin anchor

Table 6: Species of the KAN/REV network.

V.v Equations of the single cell KAN/REV network

The single cell models lacks cell to cell interactions, therefore no diffusion terms are needed.

It is also possible to discard all the signal molecules without losing any of the model dynamics. Every signal molecule would just be a copy, perhaps rescaled, of its production molecule. The only thing a signal molecule would add to the dynamics is the possibility to rescale the concentrations of the molecules appearing as repressors or activators inside the Hill functions. But this would have the same effect as changing the corresponding K's within the Hill function with the inverse factor. Hence adding a signal molecule would not lead to any new possible behaviours of the model. This being said, the single cell model equations are as follows.

KAN/REV network without KAN self-activation

$$\begin{aligned}
\frac{\mathrm{d}[R]}{\mathrm{dt}} &= V_R \frac{[A]^2}{K_{0R}^2 + [A]^2} \frac{K_{1R}^2}{K_{1R}^2 + [K]^2} - d_R[R] \\
\frac{\mathrm{d}[K]}{\mathrm{dt}} &= V_K \frac{K_{1K}^2}{K_{1K}^2 + [R]^2} - d_K[K] \\
\frac{\mathrm{d}[A]}{\mathrm{dt}} &= k_A[aA] - d_A[A]
\end{aligned} \tag{10}$$

KAN/REV network with KAN self-activation

$$\begin{aligned}
\frac{\mathrm{d}[R]}{\mathrm{dt}} &= V_R \frac{[A]^2}{K_{0R}^2 + [A]^2} \frac{K_{1R}^2}{K_{1R}^2 + [K]^2} - d_R[R] \\
\frac{\mathrm{d}[K]}{\mathrm{dt}} &= V_K \frac{[K]^2}{K_{0K}^2 + [K]^2} \frac{K_{1K}^2}{K_{1K}^2 + [R]^2} - d_K[K] \\
\frac{\mathrm{d}[A]}{\mathrm{dt}} &= k_A[aA] - d_A[A]
\end{aligned} \tag{11}$$

R	REVOLUTA
K	KANADI
mi	miRNA
A	auxin
aA	auxin anchor

Table 7: Legend for single cell full model equations.

V.vi Equations of the single cell full model

The single cell full model contains the species of the KAN/REV network, but also miRNAs (Table 7). As opposed to the multicellular model no diffusion and signal molecules are present here.

Full model without KAN self-activation

$$\begin{aligned}
\frac{\mathrm{d}[R]}{\mathrm{dt}} &= V_R \frac{[A]^2}{K_{0R}^2 + [A]^2} \frac{K_{1R}^2}{K_{1R}^2 + [K]^2} - V_{dR} \frac{[mi]^2}{K_{2R}^2 + [mi]^2} - d_R[R] \\
\frac{\mathrm{d}[K]}{\mathrm{dt}} &= k_K + V_K \frac{[K]^2}{K_{0K}^2 + [K]^2} \frac{K_{1K}^2}{K_{1K}^2 + [R]^2} - d_K[K] \\
\frac{\mathrm{d}[mi]}{\mathrm{dt}} &= V_{mi} \frac{K_{0mi}^2}{K_{0mi}^2 + [R]^2} - d_{mi}[mi] \\
\frac{\mathrm{d}[A]}{\mathrm{dt}} &= k_A[aA] - d_A[A]
\end{aligned} \tag{12}$$

Full model with KAN self-activation

$$\begin{aligned}
\frac{\mathrm{d}[R]}{\mathrm{dt}} &= V_R \frac{[A]^2}{K_{0R}^2 + [A]^2} \frac{K_{1R}^2}{K_{1R}^2 + [K]^2} - V_{dR} \frac{[mi]^2}{K_{2R}^2 + [mi]^2} - d_R[R] \\
\frac{\mathrm{d}[K]}{\mathrm{dt}} &= k_K + V_K \frac{K_{1K}^2}{K_{1K}^2 + [R]^2} - d_K[K] \\
\frac{\mathrm{d}[mi]}{\mathrm{dt}} &= V_{mi} \frac{K_{0mi}^2}{K_{0mi}^2 + [R]^2} - d_{mi}[mi] \\
\frac{\mathrm{d}[A]}{\mathrm{dt}} &= k_A[aA] - d_A[A]
\end{aligned} \tag{13}$$

V.vii Gene expressions of the anchor models

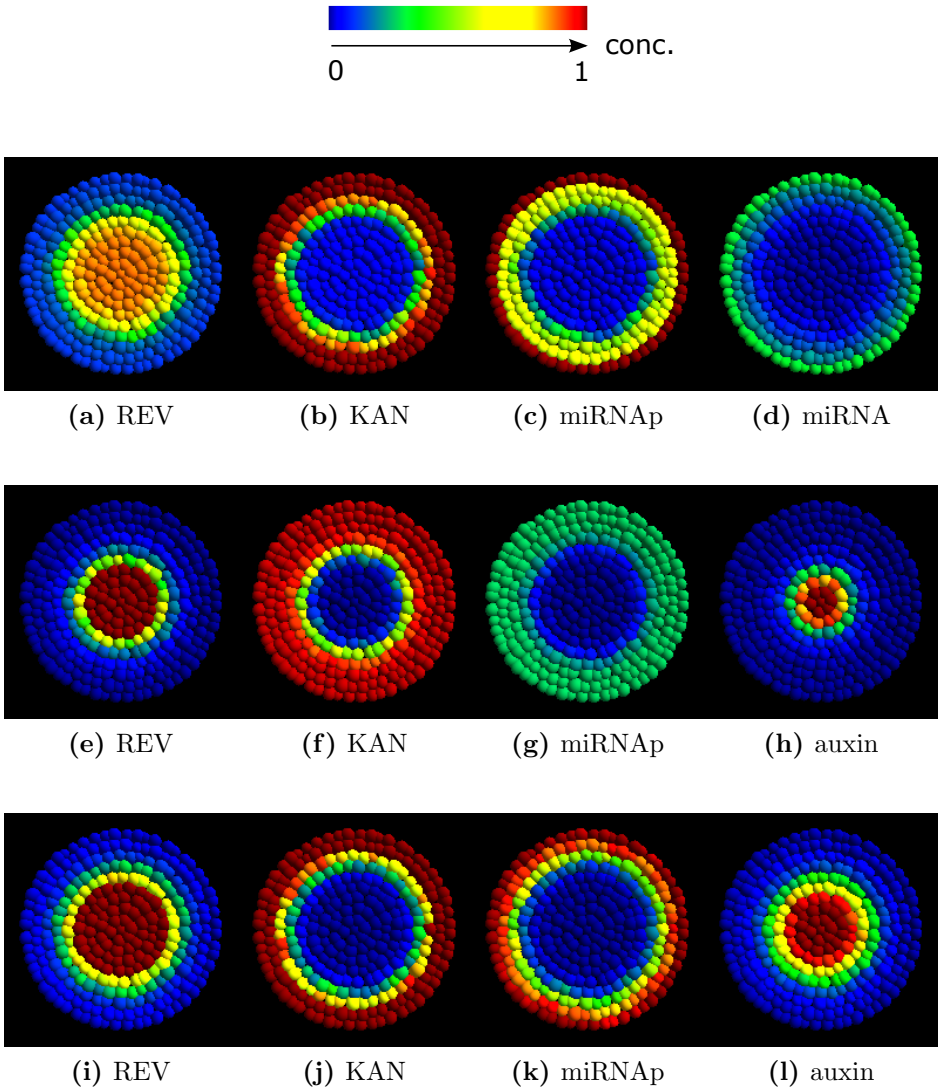

(a) REV **(b)** KAN **(c)** miRNAp **(d)** miRNA

(e) REV **(f)** KAN **(g)** miRNAp **(h)** auxin

(i) REV **(j)** KAN **(k)** miRNAp **(l)** auxin

Figure 26: Concentration levels of different molecules in the anchor models. **(a)** – **(d)** Concentration levels of the miRNA anchor model. **(e)** – **(h)** Concentration levels for the model with a small auxin anchor. **(i)** – **(l)** Concentration levels for the model with a large auxin anchor.

V.viii Model mutants gene expressions

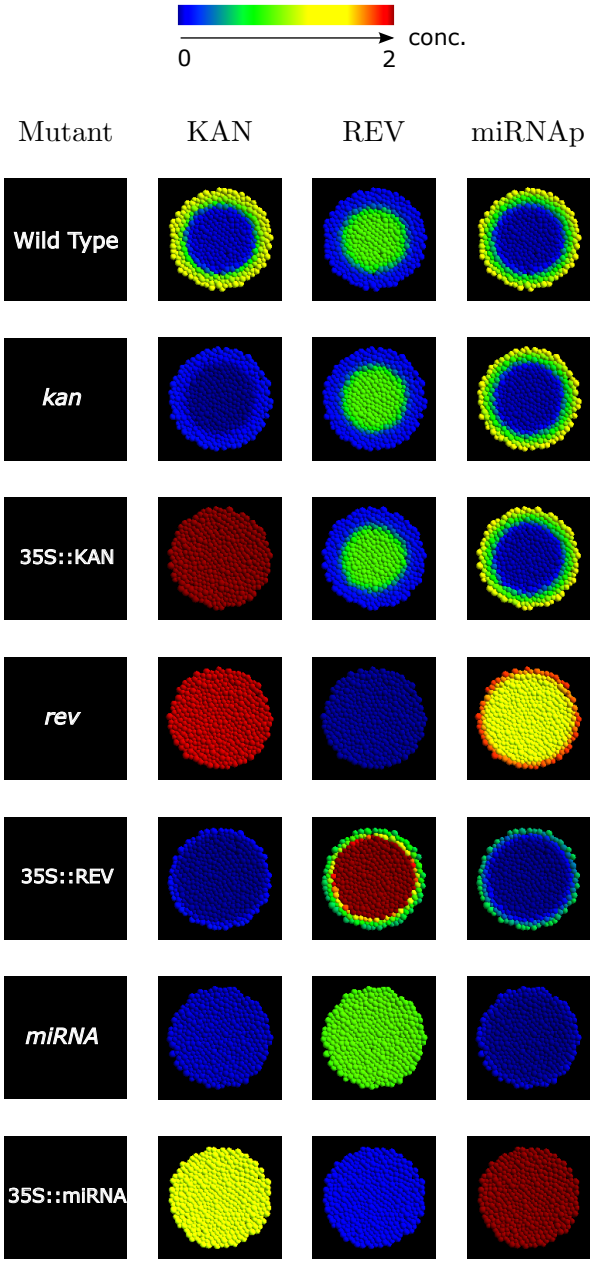

Table 8: Mutant and wild type expression levels for the model with a miRNA anchor. Each row corresponds to the mutant specified in the left-most column, and shows the relative expression of different molecules KANADI (KAN), REVOLUTA (REV) and miRNA promoter (miRNAp). Note that the *kan* and 35S::KAN mutants do not change the expression of REV or miRNA, while the other mutants effectively destroys the pattern.

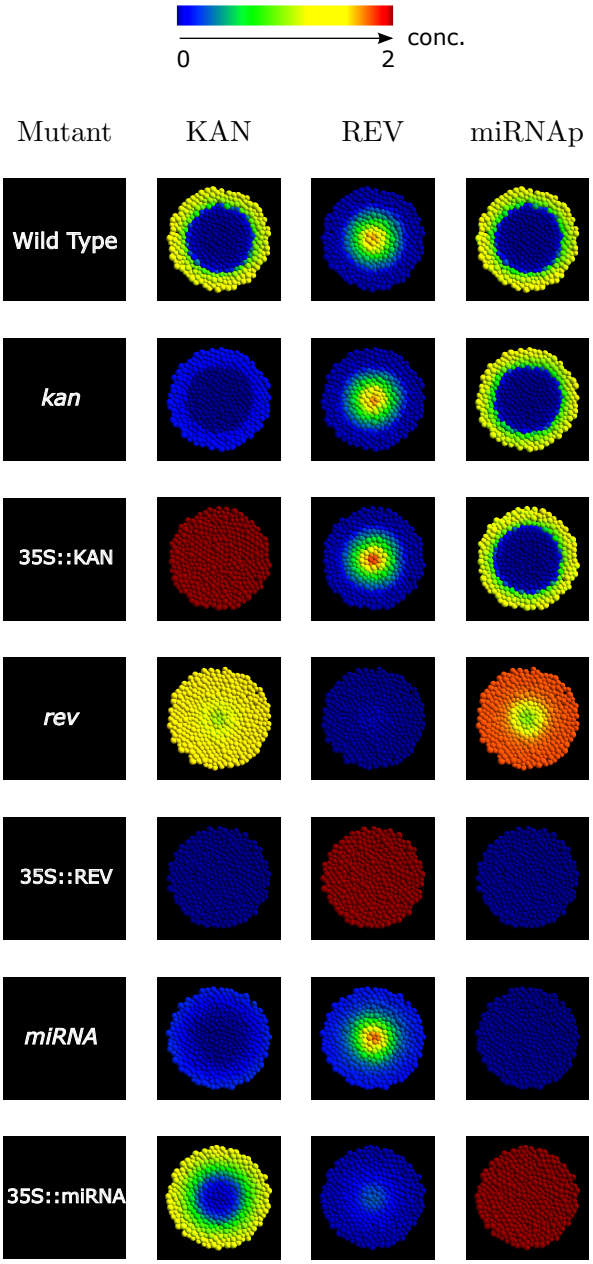

Table 9: Mutant and wild type expression levels for the model with an small auxin anchor. Each row corresponds to the mutant specified in the left-most column, and shows the relative expression of different molecules KANADI (KAN), REVOLUTA (REV) and miRNA promoter (miRNAp). Notice how the miRNA promoter is weakly expressed in the wild type expression. The miRNA/KAN mutants reveals that miRNA/KAN does not play in important part in the patterning of the SAM in this model, since the expression levels of the other species remain largely unaltered.

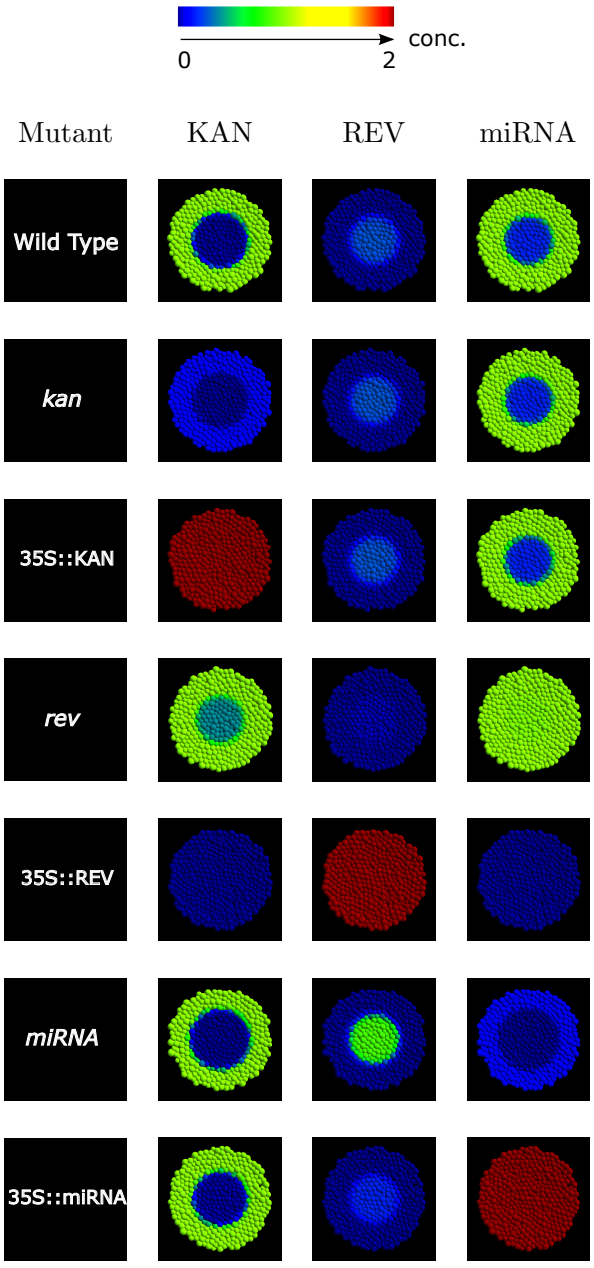

Table 10: Mutant and wild type expression levels for the model with a large auxin anchor. Each row corresponds to the mutant specified in the left-most column, and shows the relative expression of different molecules KANADI (KAN), REVOLUTA (REV) and miRNA promoter (miRNAp). Only the *REV* mutants alters the patterning of the other molecules of the model, suggesting that REV is the main determinant of the behaviour for this model.

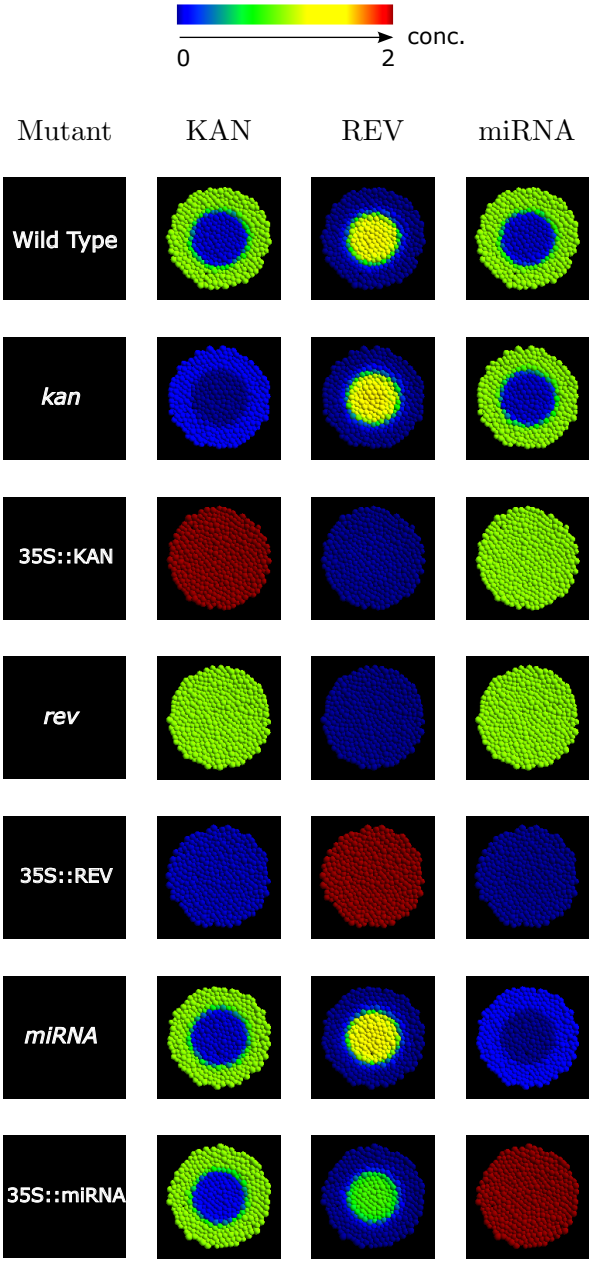

Table 11: Mutant and wild type expression levels for the full model without a self-activation of KAN. Each row corresponds to the mutant specified in the left-most column, and shows the relative expression of different molecules KAN, REVOLUTA (REV) and miRNA promoter (miRNAp).

V.ix Parameter distributions

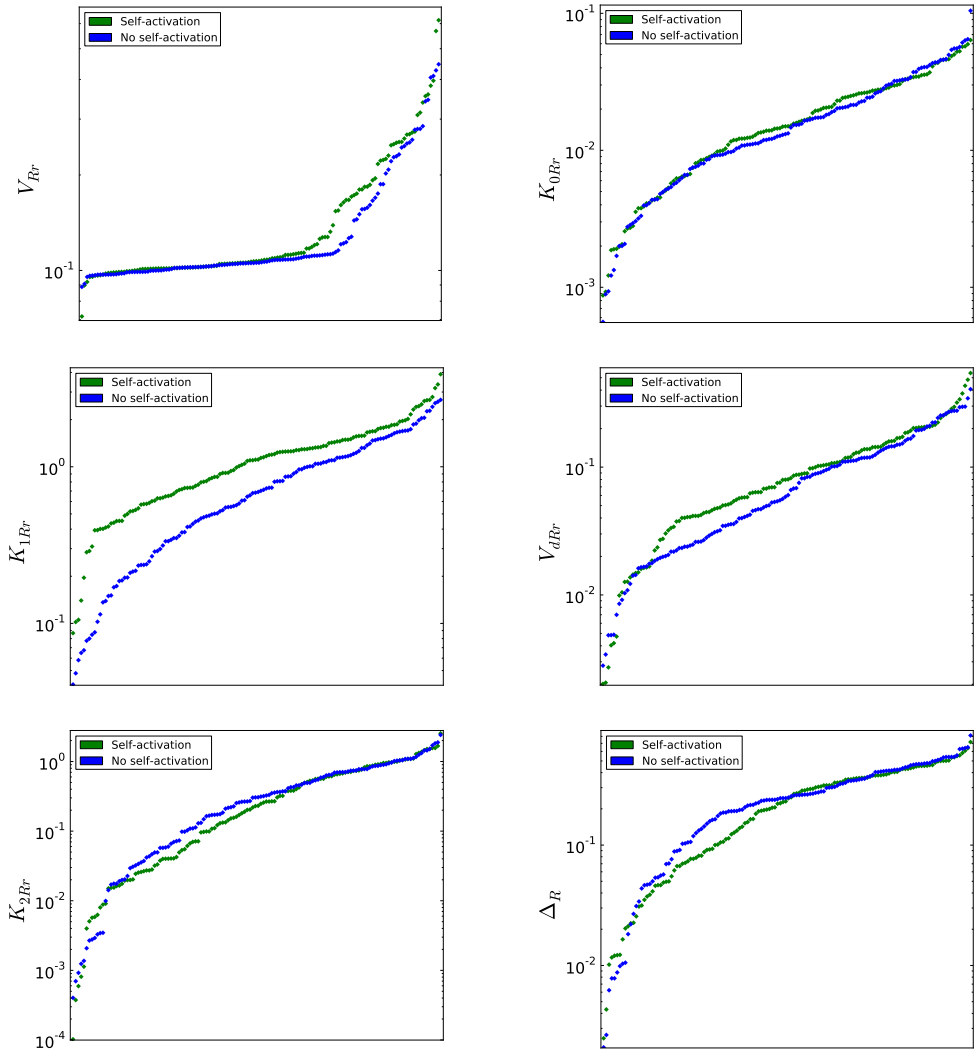

Figure 27: Plots of parameter distributions for the full model.

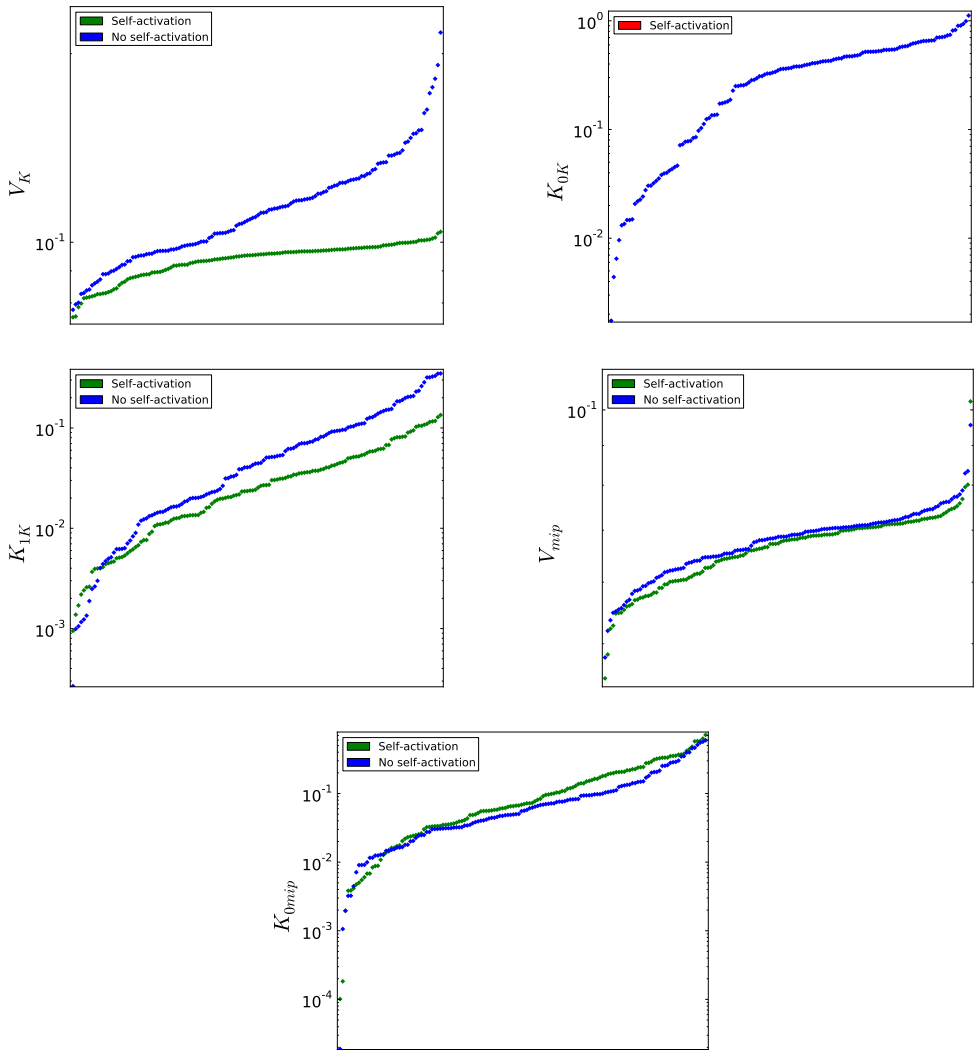

Figure 28: Plots of parameter distributions for the full model, continued.

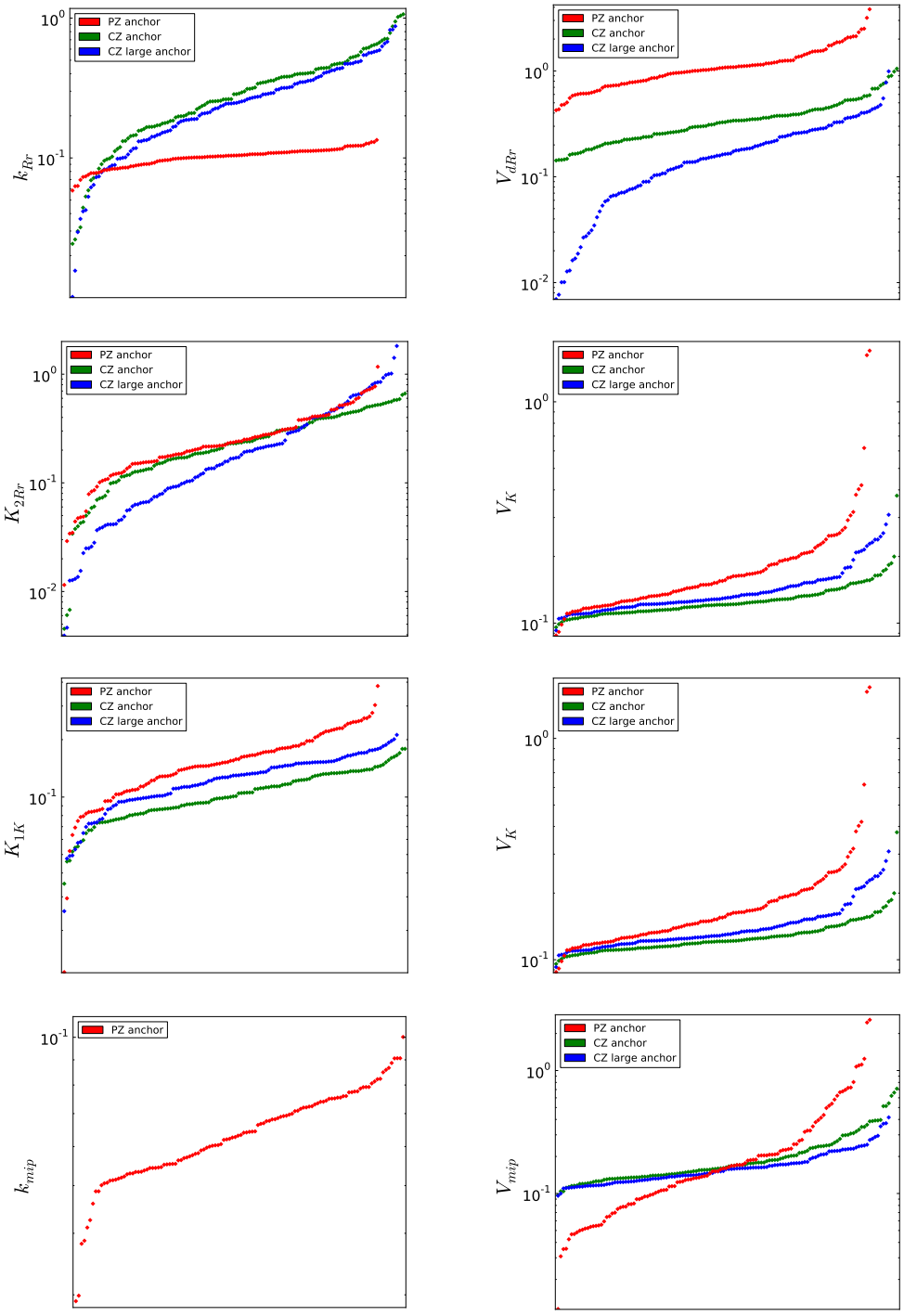

Figure 29: Plots of parameter distributions for anchor models.

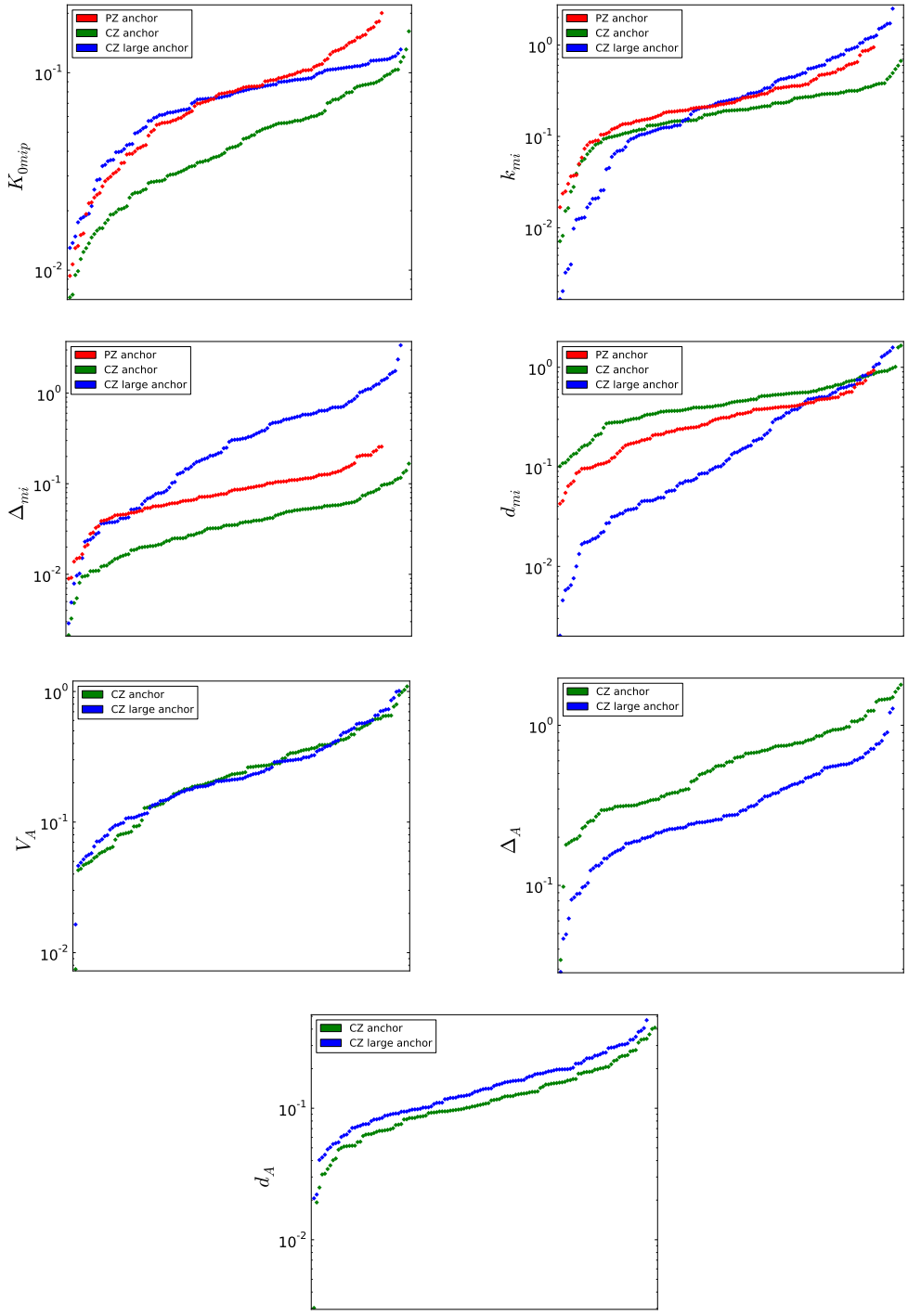

Figure 30: Plots of parameter distributions for anchor models, continued.

V.x Parameter values used in bifurcation analysis

Parameter	Value
$\not{V}_R$	1.3
K_{0R}	0.3
K_{1R}	0.3
$\not{V}_K$	1.9
K_{0K}	0.0
K_{1K}	0.3
$\alpha_{[aA]=1}$	4.0
$\alpha_{[aA]=0.1}$	0.43
β	3.3
γ	0.0

(a) KRN

Parameter	Value
$\not{V}_R$	1.2
K_{0R}	0.5
K_{1R}	0.3
$\not{V}_K$	1.1
K_{0K}	0.3
K_{1K}	0.8
$\alpha_{[aA]=1}$	1.2
$\alpha_{[aA]=0.1}$	0.058
β	3.7
γ	1.0

(b) KRN with SA

Parameter	Value
$\not{V}_R$	1.1
K_{0R}	0.2
K_{1R}	0.3
$\not{V}_{dR}$	0.7
K_{2R}	0.5
$\not{k}_K$	0.03
$\not{V}_K$	1.0
K_{0K}	0.0
K_{1K}	0.2
$\not{V}_{mi}$	1.0
K_{0mi}	0.3

(c) Full model without SA

Parameter	Value
$\not{V}_R$	1.1
K_{0R}	0.2
K_{1R}	0.2
$\not{V}_{dR}$	0.7
K_{2R}	0.5
$\not{k}_K$	0.03
$\not{V}_K$	1.05
K_{0K}	0.3
K_{1K}	0.2
$\not{V}_{mi}$	1.0
K_{0mi}	0.5

(d) Full model with SA

Table 12: Parameters used for the bifurcation plots of the single cell models, and corresponding values of dimensionless α, β, γ variables. Tables show the values for the KAN/REV network (KRN) and the full model, without and with KAN self-activation (with SA). Note that α depends on the level of auxin. Here two values of α for different levels of auxin is calculated.

V.xi Parameter values used for the *in silico* experiments

Parameter	Value
V_{Rr}	0.16
K_{0Rr}	0.2
K_{1Rr}	0.3
V_{dR}	0.07
K_{2Rr}	0.5
d_{Rr}	0.1
k_R	0.1
Δ_R	0.02
d_R	0.1
k_K	0.003
V_K	0.097
K_{1K}	0.2
d_K	0.1
V_{mip}	0.1
K_{0mip}	0.3
d_{mip}	0.1
k_{mi}	0.1
Δ_{mi}	0.05
d_{mi}	0.1
V_A	0.1
R_A/r_{cell}	6.8
k_A	0.1
d_A	0.1

(a) Full model without SA

Parameter	Value
V_{Rr}	0.12
K_{0Rr}	0.2
K_{1Rr}	0.2
V_{dR}	0.1
K_{2Rr}	0.5
d_{Rr}	0.1
k_R	0.1
Δ_R	0.01
d_R	0.1
k_K	0.003
V_K	0.1
K_{0K}	0.3
K_{1K}	0.2
d_K	0.1
V_{mip}	0.1
K_{0mip}	0.5
d_{mip}	0.1
k_{mi}	0.1
Δ_{mi}	0.05
d_{mi}	0.1
V_A	0.1
R_A/r_{cell}	6.8
k_A	0.1
d_A	0.1

(b) Full model with SA

Table 13: Parameters used for the simulations in Figure 17 and 19. Note that the parameters concerning auxin are only valid when the anchor is used rather than the *PIN1* polarisation model. The radius of the auxin anchor is measured relative to r_{cell}, the average radius of a cell.

VI Acknowledgements

I want to thank the people at the Department of Theoretical Physics in Lund involved in this work. Special thanks to H. Jönsson for support and guidance during the course of the project. I also want to thank M. Heisler and his research group for the ongoing discussions concerning relevant biological findings.

Thanks also goes to J. Gruel for showing me some python tricks, and to V. Olariu for explaining bifurcation.

References

[Adler, 1974] Adler, I. (1974). A model of contact pressure in phyllotaxis. J. theor. Biol *45*, 1–79.

[Benková et al., 2003] Benková, E., Michniewicz, M., Sauer, M., Teichmann, T., Seifertová, D., Jürgens, G. and Friml, J. (2003). Local, efflux-dependent auxin gradients as a common module for plant organ formation. Cell *115*, 591–602.

[Bilsborough et al., 2011] Bilsborough, G., Runions, A., Barkoulas, M., Jenkins, H., Hasson, A., Galinha, C., Laufs, P., Hay, A., Prusinkiewicz, P. and Tsiantis, M. (2011). Model for the regulation of Arabidopsis thaliana leaf margin development. PNAS *108*, 3424–3429.

[Brunoud et al., 2012] Brunoud, G., Wells, D., Oliva, M., Larrieu, A., Mirabet, V., Burrow, A., Beeckman, T., Kepinski, S., Traas, J., Bennett, M. et al. (2012). A novel sensor to map auxin response and distribution at high spatio-temporal resolution. Nature *482*, 103–106.

[Church, 1904] Church, A. (1904). On the relation of phyllotaxis to mechanical laws. Williams & Norgate.

[de Reuille et al., 2006] de Reuille, P., Bohn-Courseau, I., Ljung, K., Morin, H., Carraro, N., Godin, C. and Traas, J. (2006). Computer simulations reveal properties of the cell-cell signaling network at the shoot apex in Arabidopsis. PNAS *103*, 1627–1632.

[Douady and Couder, 1992] Douady, S. and Couder, Y. (1992). Phyllotaxis as a physical self-organized growth process. Phys. Rev. Lett. *68*, 2098–2101.

[Emery et al., 2003] Emery, J., Floyd, S., Alvarez, J., Eshed, Y., Hawker, N., Izhaki, A., Baum, S. and Bowman, J. (2003). Radial Patterning of Arabidopsis Shoots by Class III HD-ZIP and KANADI Genes. Current Biology *13*, 1768–1774.

[Eshed et al., 2004] Eshed, Y., Izhaki, A., Baum, S., Floyd, S. and Bowman, J. (2004). Asymmetric leaf development and blade expansion in Arabidopsis are mediated by KANADI and YABBY activities. Development *131*, 2997–3006.

[Fujita and Mochizuki, 2006] Fujita, H. and Mochizuki, A. (2006). Pattern formation of leaf veins by the positive feedback regulation between auxin flow and auxin efflux carrier. J. Theor. Biol. *241*, 541–551.

[Gälweiler et al., 1998] Gälweiler, L., Guan, C., Müller, A., Wisman, E., Mendgen, K., Yephremov, A. and Palme, K. (1998). Regulation of polar auxin transport by AtPIN1 in Arabidopsis vascular tissue. Science *282*, 2226–2230.

[Gardner et al., 2000] Gardner, T., Cantor, C. and Collins, J. (2000). Construction of a genetic toggle switch inEscherichia coli. Nature *403*, 339–342.

[Gierer and Meinhardt, 1972] Gierer, A. and Meinhardt, H. (1972). A theory of biological pattern formation. Kybernetik *12*, 30–39.

[Gruel et al., 2009] Gruel, J., LeBorgne, M., LeMeur, N. and Théret, N. (2009). In silico investigation of ADAM12 effect on TGF-β receptors trafficking. BMC research notes *2*, 193.

[Heisler et al., 2005] Heisler, M., Ohno, C., Das, P., Sieber, P., Reddy, G., Long, J. and Meyerowitz, E. (2005). Patterns of auxin transport and gene expression during primordium development revealed by live imaging of the Arabidopsis inflorescence meristem. Curr. Biol. *15*, 1899–1911.

[Hofmeister, 1868] Hofmeister, W. (1868). Allgemeine Morphologie der Gewächse, Handbuch der Physiologischen Botanik. W. Engelmann.

[Ilegems et al., 2010] Ilegems, M., Douet, V., Meylan-Bettex, M., Uyttewaal, M., Brand, L., Bowman, J. and Stieger, P. (2010). Interplay of auxin, KANADI and Class III HD-ZIP transcription factors in vascular tissue formation. Development *137*, 975–984.

[Iterson, 1907] Iterson, G. (1907). Mathematische und Mikroscopisch-Anatomische Studien über Blaltstellungen. Jena.

[Izhaki and Bowman, 2007] Izhaki, A. and Bowman, J. (2007). KANADI and class III HD-Zip gene families regulate embryo patterning and modulate auxin flow during embryogenesis in Arabidopsis. Plant Cell *19*, 495–508.

[Jönsson et al., 2005] Jönsson, H., Heisler, M., Reddy, G., Agrawal, V., Gor, V., Shapiro, B., Mjolsness, E. and Meyerowitz, E. (2005). Modeling the organization of the WUSCHEL expression domain in the shoot apical meristem. Bioinformatics *21*, i232–i240.

[Jönsson et al., 2006] Jönsson, H., Heisler, M., Shapiro, B., Meyerowitz, E. and Mjolsness, E. (2006). An auxin-driven polarized transport model for phyllotaxis. PNAS *103*, 1633–1638.

[Jönsson et al., 2004] Jönsson, H., Shapiro, B., Meyerowitz, E. and E., M., eds (2004). Modeling plant development with gene regulation networks including signaling and cell division.

[Kerstetter et al., 2001] Kerstetter, R., Bollman, K., Taylor, R., Bomblies, K. and Poethig, R. (2001). KANADI regulates organ polarity in Arabidopsis. Nature *411*, 706–709.

[Khanin and Vinciotti, 2008] Khanin, R. and Vinciotti, V. (2008). Computational modeling of post-transcriptional gene regulation by microRNAs. J Comput Biol *15*, 305–316.

[Kidner and Martienssen, 2004] Kidner, C. and Martienssen, R. (2004). Spatially restricted microRNA directs leaf polarity through ARGONAUTE1. Nature *428*, 81–84.

[Mitchison, 1977] Mitchison, G. (1977). Phyllotaxis and the Fibonacci series. Science *196*, 270–275.

[Mitchison, 1980] Mitchison, G. (1980). A model for vein formation in higher plants. Proc. R. Soc. Lond. B. *207*, 79–109.

[Otsuga et al., 2001] Otsuga, D., DeGuzman, B., Prigge, M., Drews, G. and Clark, S. (2001). REVOLUTA regulates meristem initiation at lateral positions. Plant J. *25*, 223–236.

[Reinhardt et al., 2003] Reinhardt, D., Pesce, E., Stieger, P., Mandel, T., Baltensperger, K., Bennett, M., Traas, J., Friml, J., Kuhlemeier, C. et al. (2003). Regulation of phyllotaxis by polar auxin transport. Nature *426*, 255–260.

[Rolland-Lagan and Prusinkiewicz, 2005] Rolland-Lagan, A. and Prusinkiewicz, P. (2005). Reviewing models of auxin canalization in the context of leaf vein pattern formation in Arabidopsis. Plant J. *44*, 854–865.

[Satina et al., 1940] Satina, S., Blakeslee, A. and Avery, A. (1940). Demonstration of the three germ layers in the shoot apex of Datura by means of induced polyploidy in periclinal chimeras. Am. J. Bot. *27*, 895–905.

[Schoute, 1913] Schoute, J. (1913). Beitrage zur Blattstellungslehre. I. Die Theorie., vol. 10,. Rec. des Trav. Bot.Néerland.

[Smith et al., 2006] Smith, R., Guyomarc'h, S., Mandel, T., Reinhardt, D., Kuhlemeier, C. and Prusinkiewicz, P. (2006). A plausible model of phyllotaxis. PNAS *103*, 1301–1306.

[Snow and Snow, 1932] Snow, M. and Snow, R. (1932). Experiments on phyllotaxis. I. The effect of isolating a primordium. Phil. Trans. R. Soc. Lon. B *221*, 1–43.

[Talbert et al., 1995] Talbert, P., Adler, H., Parks, D. and Comai, L. (1995). The REVOLUTA gene is necessary for apical meristem development and for limiting cell divisions in the leaves and stems of Arabidopsis thaliana. Development *121*, 2723–2735.

[Turing, 1952] Turing, A. (1952). The chemical basis of morphogenesis. Philos. Trans. R. Soc. London B *237*, 37–72.

[Veen and Lindenmayer, 1977] Veen, A. and Lindenmayer, A. (1977). Diffusion mechanism for phyllotaxis: theoretical physico-chemical and computer study. Plant Physiology *60*, 127–139.

[Vernoux et al., 2011] Vernoux, T., Brunoud, G., Farcot, E., Morin, V., Van den Daele, H., Legrand, J., Oliva, M., Das, P., Larrieu, A., Wells, D. et al. (2011). The auxin signalling network translates dynamic input into robust patterning at the shoot apex. Mol. Syst. Biol. *7*, 1–15.

[Yadav et al., 2011] Yadav, R., Perales, M., Gruel, J., Girke, T., Jönsson, H. and Reddy, G. (2011). WUSCHEL protein movement mediates stem cell homeostasis in the Arabidopsis shoot apex. Development *25*, 2025–2030.

[Yamaguchi et al., 2012] Yamaguchi, T., Nukazuka, A. and Tsukaya, H. (2012). Leaf adaxial–abaxial polarity specification and lamina outgrowth: evolution and development. Plant and Cell Physiology *53*, 1180–1194.

[Yang et al., 2006] Yang, Y., Hammes, U., Taylor, C., Schachtman, D. and Nielsen, E. (2006). High-affinity auxin transport by the AUX1 influx carrier protein. Curr. Biol. *16*, 1123–1127.

[Zito et al., 2008] Zito, T., Wilbert, N., Wiskott, L. and Berkes, P. (2008). Modular toolkit for Data Processing (MDP): a Python data processing framework. Front. neuroinform. *2*.